Structural and functional analyses of minimal phosphopeptides targeting the polo-box domain of polo-like kinase 1

Sang-Moon Yun[1,12], Tinoush Moulaei[2,12], Dan Lim[3,12], Jeong K Bang[4,12], Jung-Eun Park[1,12], Shilpa R Shenoy[5,12], Fa Liu[6], Young H Kang[1], Chenzhong Liao[6], Nak-Kyun Soung[1], Sunhee Lee[1,7], Do-Young Yoon[7], Yoongho Lim[7], Dong-Hee Lee[1,8], Akira Otaka[9], Ettore Appella[10], James B McMahon[11], Marc C Nicklaus[6], Terrence R Burke Jr[6], Michael B Yaffe[3], Alexander Wlodawer[2] & Kyung S Lee[1]

Polo-like kinase-1 (Plk1) has a pivotal role in cell proliferation and is considered a potential target for anticancer therapy. The noncatalytic polo-box domain (PBD) of Plk1 forms a phosphoepitope binding module for protein-protein interaction. Here, we report the identification of minimal phosphopeptides that specifically interact with the PBD of human PLK1, but not those of the closely related PLK2 and PLK3. Comparative binding studies and analyses of crystal structures of the PLK1 PBD in complex with the minimal phosphopeptides revealed that the C-terminal SpT dipeptide functions as a high-affinity anchor, whereas the N-terminal residues are crucial for providing specificity and affinity to the interaction. Inhibition of the PLK1 PBD by phosphothreonine mimetic peptides was sufficient to induce mitotic arrest and apoptotic cell death. The mode of interaction between the minimal peptide and PBD may provide a template for designing therapeutic agents that target PLK1.

The Plks are a conserved subfamily of serine-threonine protein kinases that have crucial roles in cell proliferation (reviewed in refs. 1,2). Plks are characterized by the presence of a highly conserved C-terminal PBD composed of the structurally related PB1 (residues 411–489 in PLK1) and PB2 (residues 511–592) motifs (reviewed in ref. 3). Multiple forms of Plks, designated Plk1, Plk2 (or Snk), Plk3 (or Prk or Fnk) and Plk4 (or Sak), exist in mammals. Plk4 is the most distantly related member of the Plk subfamily; one of the two Plk4 variants, Sak-a, contains only the PB1 motif. Among the Plks, PLK1 has been studied most extensively because of its ability to override cellular checkpoints and induce genetic instability, leading to oncogenic transformation of human cells (reviewed in refs. 4,5). Not surprisingly, PLK1 is overexpressed in a broad spectrum of human cancers. Furthermore, interference with PLK1 function induces apoptotic cell death in most tumor cells, but not in normal cells, and reduces tumor growth in mouse xenograft models (reviewed in ref. 5), suggesting that PLK1 could be targeted for therapeutic intervention against human cancers. In contrast to the role of Plk1

in cell proliferation and tumorigenesis, the two most closely related kinases, Plk2 and Plk3, seem to have a role in checkpoint-mediated cell-cycle arrest to ensure genetic stability and prevent oncogenic transformation[6,7]. Thus, specific inhibition of PLK1, but not PLK2 or PLK3, could be important for anti-Plk1 cancer therapy.

The PBD of Plk1 has a crucial role in proper subcellular localization and mitotic functions of Plk1 (refs. 8–10) by interacting with serine- or threonine-phosphorylated peptides with the invariable serine residue at the −1 position (S-p-S/T motif)[11]. Crystal structures of the PLK1 PBD in complex with artificial phosphopeptides optimized for PBD binding have revealed that the PB1 and PB2 motifs have identical β6α folds and form a heterodimeric phosphopeptide binding module[12,13]. The phosphopeptide binds to a cleft formed between PB1 and PB2 and interacts with key amino acid residues from both polo boxes. His538 and Lys540 from PB2 are pivotal for electrostatic interactions with the negatively charged phosphate group of phosphorylated serine or threonine residue, whereas Trp414 from PB1 is crucial for the selection of serine at the −1 position (referred to hereafter as Ser−1, to

[1]Laboratory of Metabolism, Center for Cancer Research, National Cancer Institute, National Institutes of Health, Bethesda, Maryland, USA. [2]Macromolecular Crystallography Laboratory, Center for Cancer Research, National Cancer Institute-Frederick, Frederick, Maryland, USA. [3]Departments of Biology and Biological Engineering, Center for Cancer Research, Massachusetts Institute of Technology, Cambridge, Massachusetts, USA. [4]Korea Basic Science Institute, Busan, South Korea. [5]Molecular Targets Development Program, SAIC-Frederick, National Cancer Institute-Frederick, Frederick, Maryland, USA. [6]Laboratory of Medicinal Chemistry, Center for Cancer Research, National Cancer Institute-Frederick, Frederick, Maryland, USA. [7]Department of Bioscience and Biotechnology, Konkuk University, Seoul, South Korea. [8]Department of Life Sciences, University of Seoul, Seoul, South Korea. [9]Graduate School of Pharmaceutical Sciences, Institute of Health Biosciences, The University of Tokushima, Tokushima, Japan. [10]Laboratory of Cell Biology, Center for Cancer Research, National Cancer Institute, National Institutes of Health, Bethesda, Maryland, USA. [11]Molecular Targets Development Program, Center for Cancer Research, National Cancer Institute-Frederick, Frederick, Maryland, USA. [12]These authors contributed equally to this work. Correspondence should be addressed to K.S.L. (kyunglee@mail.nih.gov).

Figure 1 Minimization of PBIP1 p-Thr78 peptide that binds to PLK1. (a–c) Various lengths of N-terminal Cys-(CH₂)₆–fused Thr78 peptides were cross-linked to beads (a) and then tested for their ability to precipitate PLK1 from mitotic HeLa lysates. The phosphorylated Thr78 residue ('T' in red) and the invariable Ser77 residue ('S' in blue) crucial for PBD binding are indicated in a (above right). Immunoblots with antibody to PLK1 show levels of PLK1 coprecipitated with the indicated peptides. A shortened form of the synthetic peptide optimized for PLK1 PBD binding (MQSpTPL)[13] was included for comparison. Numbers indicate efficiency of PLK1 precipitation by each peptide relative to the PLK1 signal in the input. (d) A 6-mer Thr78 peptide (LHSpTAI) analogous to the synthetic optimal peptide (MQSpTPL) was tested for PLK1 binding as in a–c.

indicate relative position from the Thr78 residue) by engaging in two hydrogen bonding interactions and van der Waals interactions with Ser–1 (refs. 12,13). However, additional elements required for achieving a highly specific interaction between human PLK1 and its binding targets remain elusive. In this study, we took multifaceted approaches to determine the elements required for the interaction. Our results may provide new insights into the development of anti-PLK1 therapeutic agents.

RESULTS

Minimal phosphopeptides for PLK1 PBD binding

PBIP1 (also known as MLF1IP, KLIP1, CENP-50 or CENP-U) was isolated as a PBD-interacting protein crucial for centromeric localization of PLK1 (ref. 14) and proper chromosome segregation[14–17]. Further investigation of the PLK1–PBIP1 interaction showed that the PBD of PLK1 binds to the Thr78 region of PBIP1 in a phosphorylation-dependent manner[14]. To better understand the binding nature of this interaction, we synthesized various Thr78-phosphorylated (p-Thr78) peptides for in vitro binding analyses. A bead-immobilized 10-mer or
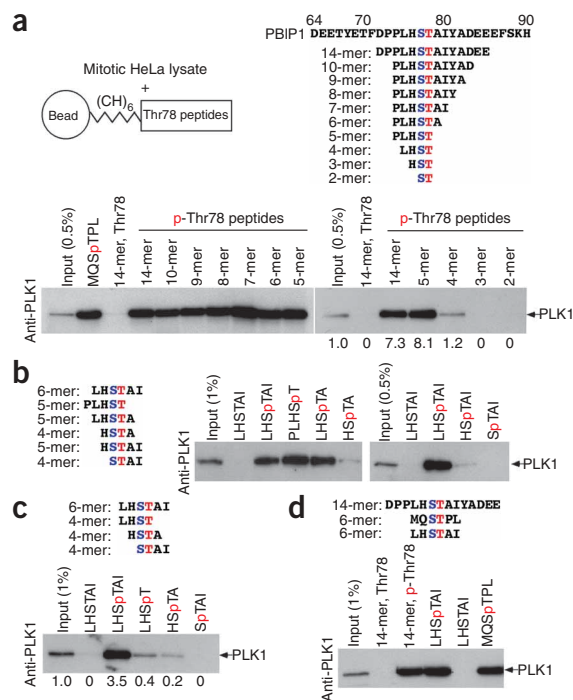
14-mer p-Thr78 peptide, but not the respective nonphosphorylated forms, precipitated PLK1 from mitotic HeLa cells as the major binding protein (**Supplementary Fig. 1a**). To determine a minimal sequence of the Thr78 motif required for the interaction, we carried out systematic deletions from the 10-mer p-Thr78 peptide (PLHSpTAIYAD) and tested the ability of various resulting peptides (**Supplementary Table 1**) to bind to PLK1. Notably, removal of all the amino acid residues C-terminal to the p-Thr78 residue did not diminish the level of PLK1 binding (**Fig. 1a**, below left), suggesting that the residues after p-Thr78 are dispensable for PBD binding. Further N-terminal deletion analyses of PLHSpT showed that the peptide LHSpT, which lacks
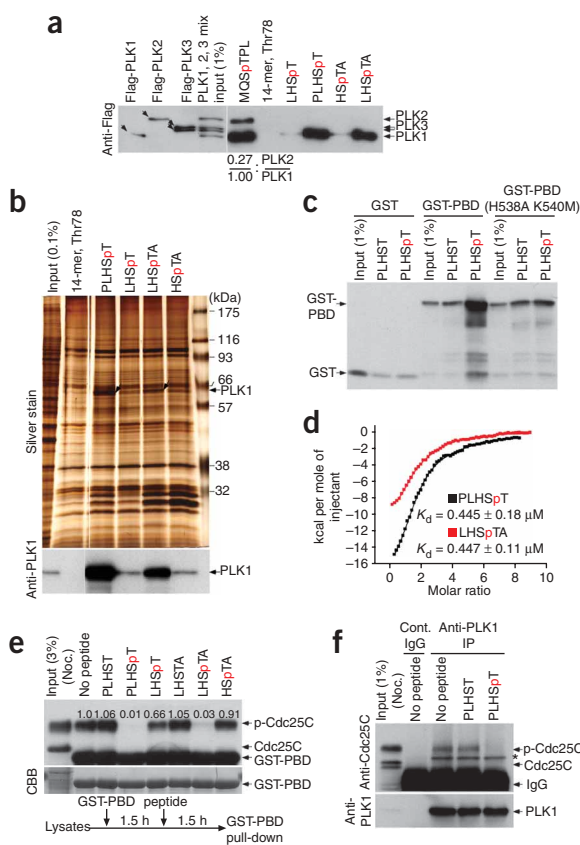

Figure 2 Minimal p-Thr78 peptides specifically bind to PLK1 with high affinity. (a) HeLa lysates expressing kinase-inactive Flag-PLK1(K82M), Flag-PLK2(K108M) or Flag-PLK3(K52R) were mixed before incubating with bead-bound Thr78 peptides or synthetic optimal peptide (MQSpTPL) as indicated and immunoblotted with antibody to Flag. PLK4 was not tested because of the distinct binding nature of its PBD. Numbers indicate fraction of PLK2 over PLK1 bound to peptide. Arrows indicate Flag-tagged PLK1, PLK2 and PLK3 proteins. (b) Mitotic HeLa lysates were incubated with the indicated bead-bound peptides. Coprecipitating proteins were analyzed by silver staining. Arrows indicate PLK1 precipitated with p-Thr78 peptides. (c) Soluble control GST, GST-PBD or GST-PBD(H538A K540M) was incubated with the indicated Thr78 peptides immobilized to beads. Bound proteins were immunoblotted with antibody to GST. (d) Isothermal titration calorimetry for p-Thr78 peptides was done using purified PLK1 PBD. Representative calorimetric isotherms for binding of two 5-mers (PLHSpT and LHSpTA) to the PBD are shown. Solid lines represent fits to the data. Overall ΔH (kcal mol⁻¹) is easily observed as the difference between the pre- and the post-binding baselines extrapolated along the y axis. (e) Mitotic HeLa lysates were preincubated with bead-bound GST-PBD for 1.5 h before addition of the indicated peptides. After another 1.5 h of incubation, GST-PBD binding proteins were precipitated and analyzed as in a. Detection of GST-PBD in the anti-Cdc25C blot is the result of previous anti-GST immunoblotting. Numbers indicate relative efficiency of p-Cdc25C pull-down by GST-PBD. CBB, Coomassie blue; Noc, nocodazole treated. (f) Mitotic HeLa lysates were treated with the indicated peptide before immunoprecipitation with either control IgG or antibody to PLK1. Immunoprecipitates were blotted with the indicated antibodies. Asterisk indicates cross-reacting protein.

Table 1 Thermodynamic binding parameters of minimal PLK1-binding peptides

Peptide	K_d (μM)	ΔH (kcal mol^{-1})	ΔS (cal mol^{-1} K^{-1})	ΔG (kcal mol^{-1})
MQSpTPL	0.534 ± 0.230	–10.01 ± 5.53	–5.24 ± 1.85	–8.55 ± 0.57
PLHSpTA	0.262 ± 0.130	–11.60 ± 3.53	–8.83 ± 1.18	–8.97 ± 0.27
LHSpTAI	0.247 ± 0.050	–11.30 ± 2.23	–7.54 ± 0.75	–9.00 ± 0.11
LHSpTA	0.447 ± 0.110	–9.90 ± 0.40	–4.19 ± 1.33	–8.65 ± 0.14
PLHSpT	0.445 ± 0.180	–14.50 ± 5.01	–19.71 ± 3.38	–8.66 ± 0.49
LHSpT	22.100 ± 0.950	–6.29 ± 2.22	–0.20 ± 0.07	–6.35 ± 0.60
HSpTA	19.500 ± 1.700	–3.82 ± 0.25	–8.70 ± 0.85	–6.42 ± 0.05
LHSTAI	No binding	No binding	No binding	No binding

the N-terminal proline, had a much lower binding affinity to PLK1, whereas HSpT, which lacks both the N-terminal proline and leucine residues, did not show any detectable level of binding (**Fig. 1a**, below right). These results suggest that PLHSpT binds to PLK1 with high affinity and that, besides the SpT dipeptide, the N-terminal Pro-Leu motif is required to provide an additional level of affinity to the PBD.

To eliminate the bias of the deletion scheme in **Figure 1a**, we also tested whether other 5-mer peptides encompassing the SpT motif bind to PLK1 efficiently. LHSpTA, which lacks the N-terminal proline but bears the C-terminal alanine, bound to PLK1 almost as efficiently as did PLHSpT (**Fig. 1b**, left). However, HSpTAI, which lacks both proline and leucine but instead bears two additional C-terminal residues after the SpT motif, bound to PLK1 only weakly (**Fig. 1b**, right), thus underlining the importance of the Leu–3 residue in the absence of the Pro–4 residue. Among the 4-mers, both LHSpT and HSpTA bound to PLK1 better than did SpTAI (**Fig. 1c**). Comparative binding studies showed that the binding affinity of a short form of the previously characterized optimal PBD binding peptide (MQSpTPL)[13] is similar to that of the analogous p-Thr78 peptide (LHSpTAI; **Fig. 1d**).

Specific, high-affinity binding of minimal p-Thr78 peptide

We tested the specificity of minimal p-Thr78 peptides against the PLK1 PBD. Similar to the initial 14-mer peptide, minimal p-Thr78 peptides precipitated PLK1 from cellular lysates containing similar levels of PLK1, PLK2 and PLK3 (**Fig. 2a** and **Supplementary Fig. 1b**). In contrast, the 6-mer optimal MQSpTPL peptide precipitated PLK2 with ~27% the efficiency of PLK1 precipitation (**Fig. 2a**), suggesting that the MQSpTPL possesses a substantially lower PLK1 specificity than does PLHSpT. Consistently, MQSpTPL, but not the p-Thr78 peptides, also precipitated PLK2 from lysates expressing PLK2 alone (**Supplementary Fig. 1c**). Notably, although much shorter than the initial 14-mer peptide, the minimal p-Thr78 peptide PLHSpT showed undiminished PLK1 specificity and precipitated PLK1 as the only major binding protein from total cellular lysates (**Fig. 2b**). Another 5-mer, LHSpTA, showed a similar but somewhat lower level of PLK1 affinity (**Fig. 2b**). These results suggest that elements crucial for PLK1-binding affinity and specificity reside within these minimal sequences. Furthermore, PLHSpT efficiently bound to glutathione S-transferase (GST)-fused PBD (GST-PBD), but not to the respective GST-PBD(H538A, K540A) phosphate pincer mutant (**Fig. 2c**), indicating that an intact phosphoepitope binding module is required for the interaction.

We next carried out isothermal titration calorimetry analyses with recombinant PLK1 PBD and quantified the binding parameters of the minimal p-Thr78 peptides. Among them, the 5-mer PLHSpT mediated the best binding contacts with the PBD ($\Delta H = -14.5$ kcal mol^{-1}; **Fig. 2d**), although its binding affinity overall (K_d ~0.45 μM) was equivalent to that of another 5-mer, LHSpTA. Under the same

conditions, the synthetic optimal 6-mer peptide, MQSpTPL, bound to PBD with a K_d of 0.534 μM (**Table 1**). Two other 6-mer peptides (PLHSpTA and LHSpTAI) had slightly higher affinities than did the 5-mer peptides, whereas two 4-mers (LHSpT and HSpTA) had much lower affinities (**Table 1**).

To test the specificity of the above peptides, we conducted calorimetry binding experiments with recombinant PLK2 PBD. Saturable binding was not observed in all cases and, as a result of the lack of a binding curve, values for binding enthalpy or binding affinity could not be extrapolated. However, a clear difference in the initial heats of interaction of the peptides was observed above the limits of detection (1 kcal mol^{-1}) of the instrument. The two minimal p-Thr78 peptides, PLHSpT and LHSpTA, showed virtually no interactions with PLK2 (only baseline heats were detected), whereas MQSpTPL titrated into PLK2 PBD produced initial heats of –1.68 kcal mol^{-1} (**Table 2**). These results corroborate the specificity of the minimal p-Thr78 peptides for PLK1 over PLK2.

p-Thr78 peptide disrupts the PBD-Cdc25C interaction

We examined whether the minimal p-Thr78 peptides have the capacity to interfere with the interaction between PLK1 PBD and its physiological binding target, phosphorylated Cdc25C (p-Cdc25C). In agreement with the previous finding, GST-PBD precipitated p-Cdc25C, but not the unphosphorylated form, from mitotic HeLa lysates[13] (**Supplementary Fig. 2a**). Addition of PLHSpT, but not the respective nonphosphorylated peptide, into the lysates disrupted the preformed PBD–p-Cdc25C complex in a phosphorylation- and concentration-dependent manner

Table 2 Peptide inhibitors of PLK1

	Pull-down assay		ITC		
Peptide[a]	PLK1 binding[b]	Plk2 binding[b]	PLK1 PBD binding[c]	Plk2 PBD binding[d]	XTAL[e]
MQSpTPL	H	M	–10.01	–1.68	Yes
DPPLHSpTAIYADEE	H	—	—	—	—
PLHSpTAIYAD	H	—	—	—	—
PLHSpTAIYA	H	—	—	—	—
PLHSpTAIY	H	—	—	—	—
PLHSpTAI	H	—	—	—	—
PLHSpTA	H	—	–11.60	—	—
PLHSpT	H	N	–14.50	No binding	Yes
LHSpT	M/L	N	–6.29	—	—
HSpT	N	—	—	—	—
SpT	N	—	—	—	—
LHSpTAI	H	N	–11.30	—	—
LHSpTA	H	N	–9.90	No binding	Yes
HSpTAI	M/L	—	—	—	—
HSpTA	M/L	N	–3.82	—	—
SpTAI	N	—	—	—	—
PAHSpT	M	N	—	—	—
PPHSpT	L	N	—	—	Yes
PQHSpT	H	L	—	—	—
PLQSpT	H	M	—	–1.10	—
PQQSpT	H	M	—	—	—
LHSTAI	N	N	No binding	—	—

[a]All peptides used for pull-down assays are fused to the N-terminal Cys-(CH$_2$)$_6$ linker, whereas all peptides used for isothermal titration calorimetry analyses are N-terminally acetylated. See **Supplementary Table 1** for details. [b]Levels of binding to PLK1 or PLK2 were categorized as high (H), moderate (M), low (L) or no or negligible (N). —, Not examined. [c]Binding enthalpy in kcal mol^{-1}, which is indicative of productive, favorable binding contacts. [d]Calorimetric initial heats of interaction in kcal mol^{-1}. [e]Crystal structure (XTAL) of PLK1 PBD-MQSpTPL complex has been described previously[12].
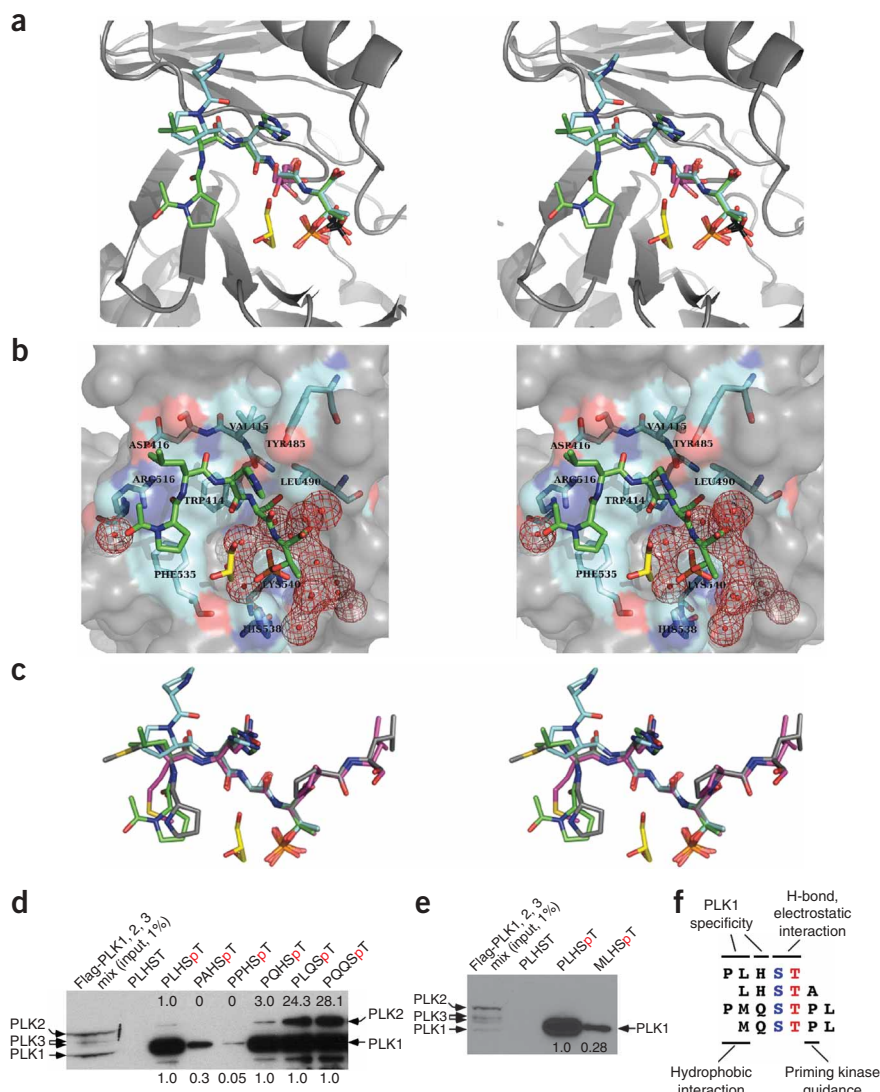The other three structures were determined in this study.

Figure 3 The nature of PBD binding and specificity. (a) Superposition of phosphopeptide binding pockets of PBD^{PL}, PBD^{PP}, PBD^{S+G} and PBD^S. Gray, PBD; green, PLHSpT; yellow, PLHSpT-associated glycerol molecule; cyan, PPHSpT; magenta, glycerol molecule (two half-occupancy conformations at Ser–1 position) of PBD^{S+G}; black, two sulfate anions of PBD^{S+G} and PBD^S (red, oxygen atoms). Differences in exact positions of sulfate and phosphate groups could result from the fact that sulfate is a free anion, whereas phosphate is covalently linked to the phosphopeptide. (b) PBD residues involved in binding of PLHSpT are labeled and shown in cyan. All water molecules that form an interface between the phosphopeptide and PBD are drawn in red mesh. (c) Superposition of PLHSpT (green), PPHSpT (cyan), MQSpTPL (magenta) and PMQSpTPL (gray). (d,e) Mixture of HeLa lysates expressing kinase-inactive Flag-PLK1(K82M), Flag-PLK2(K108M) or Flag-PLK3(K52R) was subjected to pull-down assays as in Figure 2a, with the indicated 5-mer wild-type (PLHSpT) and mutants cross-linked to beads. The nonphosphorylated Thr78 peptide PLHST was used as a control. Numbers above the blot indicate relative efficiency of PLK2 precipitation; numbers below denote relative efficiency of PLK1 precipitation. (f) Nature of interactions between SpT-containing peptides and PLK1 PBD. Alignment of minimal p-T78 peptides (PLHST and LHSTA) and synthetic optimal peptides (PMQSTPL and MQSTPL) are shown. See text for details.

peaks were modeled as sulfate, glycerol and ethylene glycol molecules. PBD^{PL} contained a glycerol molecule in the phosphopeptide binding cleft (Fig. 3a,b), occupying a cavity formed by the phosphopeptide, two water molecules and PBD. The three hydroxyl groups of this glycerol molecule were involved in hydrogen bonding with the backbone carbonyls of the phosphopeptide and PBD, the phosphate group of p-Thr, and one of the water molecules. PBD^{S+G} and PBD^S contained a sulfate anion in the same pocket (Fig. 3a), in the region normally occupied by the phosphate of p-Thr. We chose to model the density in this pocket as sulfate instead of phosphate given the presence of 0.3 M lithium sulfate in the crystallization medium. PBD^{S+G} also contained a glycerol molecule in the phosphopeptide binding cleft (Fig. 3a). This glycerol molecule was located at the −1 position, normally occupied by the serine residue when a phosphopeptide is in the binding cleft (Fig. 3a). The L2 loop in PBD^S was much less ordered than in the PBD^{S+G} structure. Analysis of contacts with symmetry-related molecules showed that this difference in the degree of order observed in the L2 region is likely to be caused by crystal packing.

Role of N-terminal residues of the minimal p-Thr78 peptides

Inspection of the structure of the PLHSpT–PBD complex revealed that, in addition to the previously described SpT-dependent interactions[12,13], the N-terminal proline residue is crucial for providing additional affinity to PBD binding by engaging in two discrete, yet interconnected, interactions. The carbonyl oxygen of the N-terminal proline residue was in polar contact (hydrogen bonding) with the guanidinium moiety of Arg516, whereas the pyrrolidine ring of the

(Supplementary Fig. 2b). In a separate experiment, LHSpTA disrupted the preformed PBD–p-Cdc25C complex nearly as efficiently as did PLHSpT, whereas both LHSpT and HSpTA disrupted the complex weakly (Fig. 2e). Furthermore, PLHSpT, but not the respective non-phosphorylated form, disrupted the in vivo PLK1–p-Cdc25C interaction (Fig. 2f). Thus, p-Thr78 peptides inhibit the interaction between the PBD and its binding targets by competitively binding to the PBD.

The binding nature of the PLK1 PBD

To investigate the binding nature of the minimal peptides to the PBD, we solved the crystal structures of the PLK1 PBD in complex with the phosphopeptides PLHSpT (hereafter referred to as PBD^{PL}) and PPHSpT (PBD^{PP}; to examine the importance of the N-terminal residue for the interaction) at 1.7-Å and at 2.3-Å resolution, respectively (Fig. 3a,b and Table 3). Additionally, we attempted to crystallize a complex by mixing the PBD (without phosphopeptide) and the kinase domain, each expressed and purified separately. However, the kinase domain precipitated, and only the PBD was found in a diffraction-quality crystal. This crystal form contained two PBD molecules per asymmetric unit, referred to as PBD^{S+G} (with sulfate and glycerol) and PBD^S (with sulfate only) for chains A and B, respectively (Fig. 3a). We found several strong peaks of positive difference density in the $F_o - F_c$ maps for PBD^{PL}, PBD^{S+G} and PBD^S, which could not be interpreted as water molecules. These

Table 3 Data collection and refinement statistics

	PBD^{PL}	PBD^S and PBD^{S+G}	PBD^{PP}	PBD^{LH}
Data collection				
Space group	$P2_12_12_1$	$P2_1$	$P2_12_12_1$	$P2_1$
Cell dimensions				
$\quad a, b, c$ (Å)	35.2, 65.8, 104.1	33.3, 102.3, 68.5	35.4, 66.5, 105.8	38.3, 62.4, 46.6
$\quad \alpha, \beta, \gamma$ (°)	90.0, 90.0, 90.0	90.0, 93.2, 90.0	90, 90, 90	90, 94.1, 90
Resolution (Å)	50.0–1.77	30.0–1.70	33.6–2.33	25.0–1.58
	(1.86–1.77)	(1.76–1.70)	(2.41–2.33)	(1.64–1.58)
R_{merge}	0.051 (0.349)	0.055 (0.259)	0.051 (0.268)	0.042 (0.172)
$I / \sigma I$	22.6 (3.6)	23.1 (2.9)	27.3 (4.9)	32.1 (8.6)
Completeness (%)	96.6 (85.0)	98.4 (85.8)	97.4 (86.5)	96.4 (94.2)
Redundancy	4.4 (4.2)	4.8 (2.9)	6.2 (5.0)	4.7 (4.5)
Refinement				
Resolution (Å)	50.0–1.77	30.0–1.70	33.6–2.33	25–1.58
No. reflections	22,482	48,194	10,186	28,941
R_{work} / R_{free}	0.205/0.237	0.187/0.219	0.246/0.293	0.189/0.229
No. atoms				
$\quad$ Protein	1,795	3,492	1,768	1,895
$\quad$ Ligand/ion	62	64	42	75
$\quad$ Water	122	325	35	262
B–factors				
$\quad$ Protein	33.7	20.4	41.7	21.7
$\quad$ Ligand/ion	36.5	36.8	39.3	18.5
$\quad$ Water	42.6	33.0	37.2	30.0
R.m.s. deviations				
$\quad$ Bond lengths (Å)	0.018	0.016	0.008	0.012
$\quad$ Bond angles (°)	1.786	1.551	1.30	1.163

Values in parentheses correspond to the highest-resolution shell.

proline residue enhanced the interaction by docking into a shallow hydrophobic pocket generated by the surrounding Trp414 and Phe535 (**Fig. 3a,b**). The importance of the latter interaction with the proline binding pocket was manifest by the observation that LHSpT, which can still form polar contact with Arg516 through the acetyl carbonyl N-terminal to the Leu–3 residue, showed ∼50-fold weaker binding than PLHSpT (**Table 1**).

We directly showed a crucial role for the N-terminal proline residue in PBD binding in experiments with PPHSpT. The N-terminal proline at the −4 position of PPHSpT was flipped out of the proline binding pocket and was unable to generate the polar contact and hydrophobic interactions because the Pro–3 residue locks the backbone of the phosphopeptide in a conformation opposite to that of PLHSpT (**Fig. 3c**). Consequently, PPHSpT showed a markedly lower (20-fold) binding affinity to PLK1 (**Fig. 3d**). Moreover, MLHSpT, bearing Met–4 instead of Pro–4, showed a much lower level of PLK1 binding (**Fig. 3e**), further highlighting the importance of the Pro–4 residue in stably binding into the pocket. Consistent with these observations, the Pro–4 residue in PMQSpTPL docked into the proline binding pocket[13] (**Fig. 3c**), whereas, in the absence of the N-terminal Pro–4, the side chain of the free (unacetylated) N-terminal Met–3 in MQSpTPL extended into the pocket[12] (**Fig. 3c**).

Notably, LHSpTA also showed a high PLK1 PBD binding affinity and specificity, even in the absence of the Pro–4 residue (**Fig. 2a,b,d**). Analyses of the crystal structure of the PLK1 PBD in complex with LHSpTA (PBD^{LH}; **Table 3**) revealed that, similar to Leu–3 of PLHSpT, the N-terminal Leu–3 side chain of LHSpTA was directed into an intramolecular cavity and did not seem to be involved in interactions with surrounding PBD residues (**Supplementary Fig. 3**). The N-terminal

acetyl carbonyl of LHSpTA was in polar contact with Arg516, thus substituting the interaction engaged by the carbonyl oxygen of the Pro–4 of PLHSpT. Because PLK2 and PLK3 possess a lysine residue at the position analogous to PLK1 Arg516, the polar contact observed in the two PLK1-specific peptides, PLHSpT and LHSpTA, is likely to be one of the major determinants of PLK1 PBD specificity.

Apart from the phosphopeptide backbone region of Leu–3, as mentioned above, the weak electron density ($2F_o − F_c$) observed in the PBD^{PL} structure (**Supplementary Fig. 4**) suggested that the leucine side chain region is disordered and may not be involved in interactions with PBD. However, mutation of the Leu–3 of PLHSpT to alanine greatly diminished the level of PLK1 binding, whereas mutation to glutamine did not alter the PLK1 affinity (**Fig. 3d**).
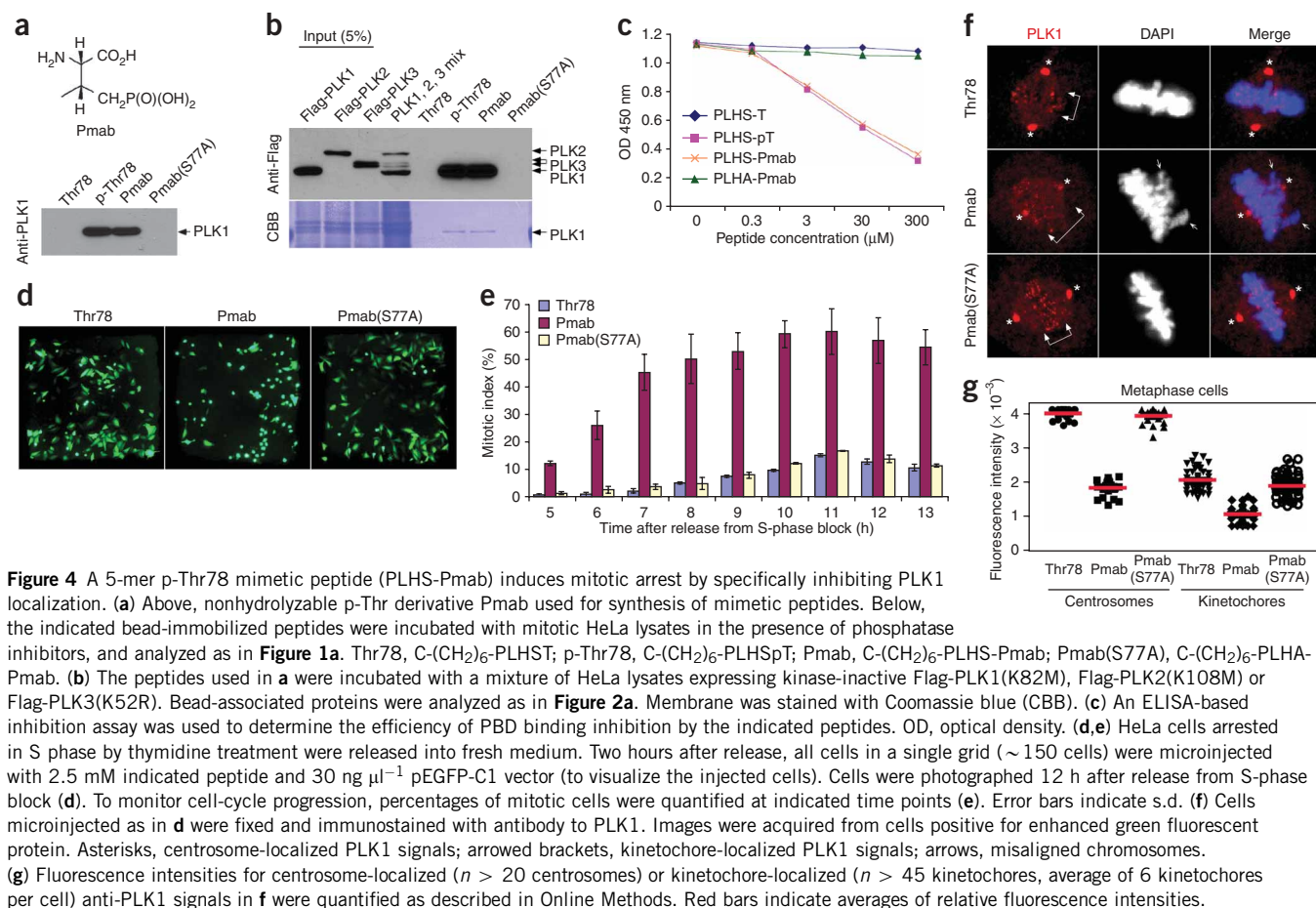
We next examined the importance of the His–2 residue for PLK1 specificity. In the crystal structure, the side chain of the His–2 residue did not directly mediate contacts with PBD residues (**Fig. 3a,b**). Notably, mutation of His–2 to glutamine substantially increased (24-fold) the level of PLK2 binding (**Fig. 3d**). In calorimetry experiments, titration of the PLQSpT mutant into PLK2 PBD produced initial heats of interaction on the order of −1.1 kcal mol$^{−1}$, compared to virtually baseline heats for the parent PLHSpT (**Table 2**). This finding suggests that the mutant peptide mediates binding contacts with PLK2 PBD, whereas the parent peptide is selective only for PLK1 PBD.

Our results suggest that the N-terminal Pro-Leu motif at the −4 and −3 positions is crucial for high-affinity and high-specificity interactions with PLK1 PBD, whereas the histidine residue at the −2 position is important to assure an additional layer of PLK1 specificity (**Fig. 3f**). These findings explain in part why MQSpTPL, bearing the N-terminal methionine for the proline binding pocket and lacking the crucial His–2 residue, has a low PLK1 specificity. In addition, the Thr78 residue in PBIP1 is followed by alanine in place of the commonly found proline residue, thus allowing a non–proline-directed kinase such as PLK1 to phosphorylate the Thr78 residue (**Fig. 3f**).

Inhibition of PLK1 PBD function by p-Thr78 mimetic peptide
The PBD-dependent interactions with various S-p-S/T–containing targets are crucial for proper PLK1 localization. As expected, acute inhibition of CDC2, one of the major kinases that prime the PBD-binding sites, markedly diminished the level of PLK1 localization to the centrosomes and kinetochores in prometaphase cells (**Supplementary Fig. 5**). This observation prompted us to test whether the minimal p-Thr78 peptides can interfere with the function of PLK1 by disrupting its localization *in vivo*. Consistent with the PBD pull-down assays, PLHSpT, but not the respective nonphosphorylated peptide, efficiently inhibited the p-Thr78–dependent PBD interaction *in vitro*, whereas LHSpTA inhibited the PBD at a moderately lower level (**Supplementary Fig. 6**). Because the phosphate group of the Thr78 residue is strictly required for PBD binding but is susceptible to dephosphorylation by intracellular phosphatases, we synthesized a phosphatase-resistant p-Thr

Figure 4 A 5-mer p-Thr78 mimetic peptide (PLHS-Pmab) induces mitotic arrest by specifically inhibiting PLK1 localization. (**a**) Above, nonhydrolyzable p-Thr derivative Pmab used for synthesis of mimetic peptides. Below, the indicated bead-immobilized peptides were incubated with mitotic HeLa lysates in the presence of phosphatase inhibitors, and analyzed as in **Figure 1a**. Thr78, C-(CH$_2$)$_6$-PLHST; p-Thr78, C-(CH$_2$)$_6$-PLHSpT; Pmab, C-(CH$_2$)$_6$-PLHS-Pmab; Pmab(S77A), C-(CH$_2$)$_6$-PLHA-Pmab. (**b**) The peptides used in **a** were incubated with a mixture of HeLa lysates expressing kinase-inactive Flag-PLK1(K82M), Flag-PLK2(K108M) or Flag-PLK3(K52R). Bead-associated proteins were analyzed as in **Figure 2a**. Membrane was stained with Coomassie blue (CBB). (**c**) An ELISA-based inhibition assay was used to determine the efficiency of PBD binding inhibition by the indicated peptides. OD, optical density. (**d,e**) HeLa cells arrested in S phase by thymidine treatment were released into fresh medium. Two hours after release, all cells in a single grid (~150 cells) were microinjected with 2.5 mM indicated peptide and 30 ng μl^{-1} pEGFP-C1 vector (to visualize the injected cells). Cells were photographed 12 h after release from S-phase block (**d**). To monitor cell-cycle progression, percentages of mitotic cells were quantified at indicated time points (**e**). Error bars indicate s.d. (**f**) Cells microinjected as in **d** were fixed and immunostained with antibody to PLK1. Images were acquired from cells positive for enhanced green fluorescent protein. Asterisks, centrosome-localized PLK1 signals; arrowed brackets, kinetochore-localized PLK1 signals; arrows, misaligned chromosomes. (**g**) Fluorescence intensities for centrosome-localized (*n* > 20 centrosomes) or kinetochore-localized (*n* > 45 kinetochores, average of 6 kinetochores per cell) anti-PLK1 signals in **f** were quantified as described in Online Methods. Red bars indicate averages of relative fluorescence intensities.

mimetic, (2S,3R)-2-amino-3-methyl-4-phosphonobutyric acid (Pmab), in protected form and incorporated it into peptides in place of the p-Thr residue (**Fig. 4a**). The bead-immobilized PLHS-Pmab precipitated PLK1, but not PLK2 or PLK3, from mitotic HeLa lysates as efficiently as did the PLHSpT peptide (**Fig. 4a,b**). As would be expected if the binding were PBD dependent, a mutation of the invariably required Ser–1 residue to alanine (PLHA-Pmab; hereafter Pmab(S77A) for simplicity) abolished PLK1 binding. Furthermore, the PLHS-Pmab peptide, but not the Pmab(S77A) mutant, efficiently interfered with p-Thr78–dependent PLK1 PBD interaction (**Fig. 4c**).

To examine the effect of the Pmab-containing mimetic peptide *in vivo*, and to overcome poor membrane permeability of a negatively charged peptide, we conducted microinjection studies using HeLa cells released from an S-phase block. As would be expected if the function of PLK1 PBD were inhibited, the Pmab peptide, but not the Pmab(S77A) or nonphosphorylated Thr78 peptides, induced mitotic arrest in ~60% of the microinjected cells (**Fig. 4d,e**). Reminiscent of the phenotype associated with loss of PBD function[10,18], ~25% of the arrested population (*n* > 180 cells) showed a chromosome congression defect (**Fig. 4f**). Owing to the increasing level of apoptotic cell death after a prolonged mitotic block, the total numbers of arrested cells began to shrink at later time points (**Fig. 4e**). Consistent with these observations, the Pmab peptide, but not the Pmab(S77A) or nonphosphorylated Thr78 peptides, interfered with PLK1 localization at the centrosomes and kinetochores and diminished PLK1 fluorescence signals (**Fig. 4f,g**) to a level similar to that observed after treatment with the CDC2 inhibitor BMI-1026 (**Supplementary Fig. 5**). Although not as efficient as the

PLHS-Pmab peptide, another type of 2-amino-4,4-difluoro-3-methyl-4-phosphobutanoic acid (F$_2$Pmab)-containing mimetic, PLHS-F$_2$Pmab-A, but not the respective F$_2$Pmab(S77A) mutant, precipitated PLK1 (**Supplementary Fig. 7a**) and induced PLK1 delocalization and chromosome misalignment that led to mitotic arrest and apoptotic cell death (**Supplementary Fig. 7b–f**). These results indicate that inhibition of PBD by the p-Thr78 mimetic peptide is sufficient to interfere with subcellular localization and mitotic functions of PLK1.

DISCUSSION

PLK1 overexpression is closely associated with tumorigenesis in a wide range of human cancers. It is also associated with aggressive disease stage and poor patient survival in various types of cancers[5], suggesting that PLK1 is a potential target for anticancer therapies. Over the years, efforts have been made to generate PLK1 inhibitors, resulting in several compounds (Boehringer Ingelheim 2536, GlaxoSmithKline compound 1, cyclapolin 1, DAP81 and ZK-thiazolidinone) developed to competitively inhibit the kinase activity of PLK1 (ref. 5). However, largely because of the structural similarities among the catalytic domains of all Plks and other related kinases, it has been difficult to generate PLK1-specific inhibitors. Because the noncatalytic PBD is found only in members of the Plk subfamily, development of inhibitors that target the PBD of PLK1 may be an alternative strategy for selectively targeting PLK1.

In conducting studies on the interaction between PLK1 and its physiological binding target, PBIP1, we identified minimal phosphopeptides derived from the Thr78 region of PBIP1 that show a high

level of affinity and specificity for the PLK1 PBD. Similar to the defects associated with the expression of a dominant-negative PBD[10,18], inhibition of the PLK1 PBD function by nonhydrolyzable p-Thr78 mimetic peptides induced a chromosome congression defect that led to mitotic arrest and apoptotic cell death. Because interference with PLK1 function induces apoptosis in most tumor cells, but not in normal cells[5], these findings suggest that inhibition of the PBD function is sufficient to interfere with tumor cell proliferation. Furthermore, our results provide the proof of principle that specific inhibition of PLK1 PBD is achievable by small mimetic peptides or their relevant compounds.

SpT-dependent electrostatic interactions are crucial for the binding of optimal peptides (PMQSpTPL and MQSpTPL) to the PLK1 PBD[12,13]. Comparative *in vitro* binding studies and analyses of the phosphopeptide binding pockets of PBD^{S+G} and PBD^S with PBD^{PL}, PBD^{PP} and PBD^{LH} revealed that, in addition to the SpT motif of the phosphopeptide acting as a high-affinity anchor, the N-terminal residues provide additional binding affinity and specificity to the PLK1 PBD through at least three distinct interactions. First, the polar contact between the carbonyl oxygen N-terminal to the Leu−3 of PLHSpT or LHSpTA and the guanidinium moiety of Arg516 of PLK1 PBD provides a molecular basis for a high-affinity and high-specificity interaction. Unlike PLK1, both PLK2 and PLK3 possess a lysine residue (Lys607 and Lys568, respectively) at the position analogous to the PLK1 Arg516. Second, docking of the N-terminal Pro−4 side chain into the pocket generated by the surrounding Trp414 and Phe535 offers additional affinity and, probably, another layer of specificity to the interaction. The PBDs from both PLK2 and PLK3 possess lysine and tyrosine residues at positions corresponding to the PLK1 Arg516 and Phe535 residues, respectively; as a consequence, they may be unable to generate as favorable an environment to accommodate the N-terminal proline residue. Third, mutational analyses of PLHSpT suggest that the His−2 residue is also crucial in determining PLK1 PBD specificity. Because the Nδ1 of His−2 was involved in a hydrogen bond with the carbonyl oxygen of Ser−1, one possibility is that the hydrogen bond between these two residues is important for conferring PLK1 specificity. Alternatively, the presence of a glutamine residue at the −2 position could be crucial for strong Plk2-mediated interactions.

Besides each amino acid residue of the p-Thr78 peptide involved in defining the PLK1 PBD binding, the positions of the glycerol in the neighboring pocket and the network of water molecules that mediate contacts between the phosphopeptide and the PBD suggest that both the glycerol and the water molecules surrounding the phosphopeptide are important elements of PBD recognition by phosphopeptides. Furthermore, the structures of PBD^{S+G}, PBD^S, PBD^{PL} and PBD^{LH} were remarkably similar, hinting that the glycerol molecule and the sulfate anion that occupy the phosphopeptide binding cleft mimic the role of the SpT dipeptide.

In conclusion, our results indicate that the PLK1 PBD binding pocket accommodates (i) the core SpT motif, (ii) the N-terminal hydrophobic residue, (iii) glycerol and (iv) a network of contacting water molecules. A combination of some or all of these four elements could be used for targeted drug design. A better understanding of PBD interaction, as well as further isolation and development of PBD binding agents, would greatly facilitate the discovery of a new class of PLK1-specific anticancer therapeutic agents.

METHODS

Methods and any associated references are available in the online version of the paper at http://www.nature.com/nsmb/.

Accession codes. Protein Data Bank: Coordinates for PBD^{PL}, PBD^{PP} and PBD^{LH} have been deposited under accession codes 3HIK, 3C5L and 3FVH, respectively; coordinates for PBD^S and PBD^{S+G} have been deposited under accession code 3HIH.

Note: Supplementary information is available on the Nature Structural & Molecular Biology website.

AUTHOR CONTRIBUTIONS
K.S.L., T.M., D.L., J.-E.P., S.R.S., F.L., Y.H.K., A.W., M.B.Y. and T.R.B. designed the experiments; S.-M.Y., T.M., D.L., J.K.B., J.-E.P., S.R.S., F.L., Y.H.K., C.L., N.-K.S. and S.L. conducted the experiments; K.S.L., T.M., D.L., S.R.S., A.W., M.B.Y., T.R.B., J.B.M., D.-H.L., M.C.N., E.A., A.O., D.-Y.Y. and Y.L. analyzed the data; and K.S.L., T.M., D.L., S.R.S., A.W., M.B.Y., F.L. and T.R.B. wrote the paper.

Published online at http://www.nature.com/nsmb/.
Reprints and permissions information is available online at http://npg.nature.com/reprintsandpermissions/.

1. Barr, F.A., Sillje, H.H. & Nigg, E.A. Polo-like kinases and the orchestration of cell division. *Nat. Rev. Mol. Cell Biol.* **5**, 429–440 (2004).
2. van de Weerdt, B.C. & Medema, R.H. Polo-like kinases: a team in control of the division. *Cell Cycle* **5**, 853–864 (2006).
3. Lowery, D.M., Lim, D. & Yaffe, M.B. Structure and function of polo-like kinases. *Oncogene* **24**, 248–259 (2005).
4. Eckerdt, F., Yuan, J. & Strebhardt, K. Polo-like kinases and oncogenesis. *Oncogene* **24**, 267–276 (2005).
5. Strebhardt, K. & Ullrich, A. Targeting polo-like kinase 1 for cancer therapy. *Nat. Rev. Cancer* **6**, 321–330 (2006).
6. Burns, T.F., Fei, P., Scata, K.A., Dicker, D.T. & El-Deiry, W.S. Silencing of the novel p53 target gene Snk/Plk2 leads to mitotic catastrophe in paclitaxel (taxol)-exposed cells. *Mol. Cell. Biol.* **23**, 5556–5571 (2003).
7. Xie, S., Xie, B., Lee, M.Y. & Dai, W. Regulation of cell cycle checkpoints by polo-like kinases. *Oncogene* **24**, 277–286 (2005).
8. Jang, Y.J., Lin, C.Y., Ma, S. & Erikson, R.L. Functional studies on the role of the C-terminal domain of mammalian polo-like kinase. *Proc. Natl. Acad. Sci. USA* **99**, 1984–1989 (2002).
9. Lee, K.S., Grenfell, T.Z., Yarm, F.R. & Erikson, R.L. Mutation of the polo-box disrupts localization and mitotic functions of the mammalian polo kinase Plk. *Proc. Natl. Acad. Sci. USA* **95**, 9301–9306 (1998).
10. Seong, Y.S. *et al.* A spindle checkpoint arrest and a cytokinesis failure by the dominant-negative polo-box domain of Plk1 in U-2 OS cells. *J. Biol. Chem.* **277**, 32282–32293 (2002).
11. Elia, A.E., Cantley, L.C. & Yaffe, M.B. Proteomic screen finds pSer/pThr-binding domain localizing Plk1 to mitotic substrates. *Science* **299**, 1228–1231 (2003).
12. Cheng, K.Y., Lowe, E.D., Sinclair, J., Nigg, E.A. & Johnson, L.N. The crystal structure of the human polo-like kinase-1 polo box domain and its phospho-peptide complex. *EMBO J.* **22**, 5757–5768 (2003).
13. Elia, A.E. *et al.* The molecular basis for phospho-dependent substrate targeting and regulation of Plks by the polo-box domain. *Cell* **115**, 83–95 (2003).
14. Kang, Y.H. *et al.* Self-regulation of Plk1 recruitment to the kinetochores is critical for chromosome congression and spindle checkpoint signaling. *Mol. Cell* **24**, 409–422 (2006).
15. Minoshima, Y. *et al.* The constitutive centromere component CENP-50 is required for recovery from spindle damage. *Mol. Cell. Biol.* **25**, 10315–10328 (2005).
16. Foltz, D.R. *et al.* The human CENP-A centromeric nucleosome-associated complex. *Nat. Cell Biol.* **8**, 458–469 (2006).
17. Okada, M. *et al.* The CENP-H-I complex is required for the efficient incorporation of newly synthesized CENP-A into centromeres. *Nat. Cell Biol.* **8**, 446–457 (2006).
18. Hanisch, A., Wehner, A., Nigg, E.A. & Sillje, H.H. Different Plk1 functions show distinct dependencies on Polo-Box domain-mediated targeting. *Mol. Biol. Cell* **17**, 448–459 (2006).

ONLINE METHODS

Peptide synthesis. The peptides used in this study are shown in **Supplementary Table 1**. We synthesized the peptides using a 9-fluorenylmethoxycarbony (Fmoc)-based solid-phase method on Rink amide resin (0.36 mmol g^{-1}; Novabiochem) at the 0.1-mmol scale. Briefly, Fmoc-protected amino acids (2.5-fold molar excess) were sequentially condensed using 0.25 mmol of N,N'-diisopropylcarbodiimide-N-hydroxybenzotriazole dissolved in dimethylformamide. Fmoc deprotection was achieved by 20% v/v piperidine/N-methylpyrrolidinone. The synthesis of protected Pmab and its incorporation into peptides will be reported separately. For peptide-based pull-down assays, peptides bearing the N-terminal Cys-$(CH_2)_6$ linkers (1 mM stock) were cross-linked to the beads using SulfoLink coupling gel (Pierce).

Peptide pull-down, GST-PBD pull-down and PBD-binding inhibition assays. Peptide and GST-PBD pull-down assays were done as described previously[14]. An ELISA-based PBD-binding inhibition assay was carried out using an immobilized p-Thr78 peptide and cellular lysates expressing hemagglutinin-tagged EGFP-PLK1. Further details are provided in **Supplementary Methods**.

Isothermal titration calorimetry analyses. Calorimetric titrations were carried out using purified recombinant PBDs (for PLK1 and PLK2) from bacterial cells and the indicated peptides. Further details are provided in **Supplementary Methods**.

Cloning, protein expression and purification. Details of PBD construction, expression and purification are described in **Supplementary Methods**.

Crystallization, data collection and refinement for PBD^{PL} and PBD^{PP}. All initial crystallization screens for the PLK1 PBD–PLHSpT complex were done on an Art Robbins Phoenix liquid handling system using Index (Hampton Research) and PEG (Qiagen) crystallization kits. All subsequent crystals were grown using the hanging-drop vapor diffusion method at room temperature (20 °C). PBD and the kinase domain of PLK1 were concentrated to $\sim$30 mg ml^{-1} in buffer A (20 mM Tris-Cl (pH 8.0), 500 mM NaCl and 3 mM DTT). The acetylated phosphopeptide Ac-PLHSpT was dissolved in buffer A. The phosphopeptide and PBD were added in a 2:1 stoichiometric ratio, respectively, and the final concentration was adjusted to $\sim$15 mg ml^{-1}. Crystals of this complex were grown by adding 1 μl of this complex to 1 μl of well solution (0.2 M di-potassium phosphate and 20% (w/v) PEG 3350). The complex between PBD and kinase domain was formed similarly using a 1:1 stoichiometric ratio and

well solution (0.2 M lithium sulfate monohydrate, 0.1 M Bis-Tris (pH 5.5) and 25% (w/v) PEG 3350). Crystals formed within 1 week and were soaked for 5 min in mother liquor constituted with 20% (v/v) glycerol before being flash-frozen in liquid nitrogen. The complex of PBD and Ac-PLHSpT crystallized in the space group $P2_12_12_1$ (a = 35.19 Å, b = 65.76 Å, c = 104.11 Å). The kinase domain of PLK1 precipitated and PBD crystallized in the space group $P2_1$ (a = 35.29 Å, b = 102.29 Å, c = 68.55 Å, β = 93.24°).

Crystals of the PLK1 PBD–PPHSpT complex were obtained in a similar fashion using a well solution of 0.1 M MES buffer (pH 6.0) containing 15% (w/v) PEG 3350. The crystals were soaked for 5 min in the mother liquor constituted with 15% (v/v) glycerol, 10 mM DTT and 2 mM phosphopeptide Ac-PPHSpT before being frozen in liquid nitrogen. This complex crystallized in the space group $P2_12_12_1$ (a = 35.44 Å, b = 66.50 Å, c = 105.82 Å). All data were collected at 100 K. The data for PBD and PBD in complex with Ac-PLHSpT were collected at the SER-CAT beamline 22-ID, at the Advanced Photon Source (Argonne National Laboratory), on a MAR 300CCD detector. The data for the complex of PBD and Ac-PPHSpT were collected at Advanced Photon Source beamline 24-ID-C at 100 K. All data were processed and scaled using the HKL2000 package[19]. Phasing of the data was done by molecular replacement using a previously published structure (PDB 1UMW)[20]. The structures were refined independent of each other with REFMAC5 (ref. 21) and CNS1.1 (ref. 22). Model building was done using Coot[23] and XtalView[24] (**Table 3**).

Cell culture, microinjection and confocal microscopy. Detailed information on cell culture, microinjection and confocal microscopy procedures are provided in **Supplementary Methods**.

19. Otwinowski, Z. & Minor, W. Processing of X-ray diffraction data collected in oscillation mode. *Methods Enzymol.* **276**, 307–326 (1997).
20. Elia, A.E. *et al.* The molecular basis for phospho-dependent substrate targeting and regulation of Plks by the polo-box domain. *Cell* **115**, 83–95 (2003).
21. Murshudov, G.N., Vagin, A.A. & Dodson, E.J. Refinement of macromolecular structures by the maximum-likelihood method. *Acta Crystallogr. D Biol. Crystallogr.* **53**, 240–255 (1997).
22. Brünger, A.T. *et al.* Crystallography & NMR system: A new software suite for macromolecular structure determination. *Acta Crystallogr. D Biol. Crystallogr.* **54**, 905–921 (1998).
23. Emsley, P. & Cowtan, K. Coot: model-building tools for molecular graphics. *Acta Crystallogr. D Biol. Crystallogr.* **60**, 2126–2132 (2004).
24. McRee, D.E. XtalView/Xfit–A versatile program for manipulating atomic coordinates and electron density. *J. Struct. Biol.* **125**, 156–165 (1999).

ONLINE SUPPLEMENTAL MATERIALS

Structural and functional analyses of minimal phosphopeptides targeting the polo-box domain of polo-like kinase 1

Sang-Moon Yun, Tinoush Moulaei, Dan Lim, Jeong K. Bang, Jung-Eun Park, Shilpa R. Shenoy, Fa Liu, Young Hwi Kang, Chenzhong Liao, Nak-Kyun Soung, Sunhee Lee, Do-Young Yoon, Yoongho Lim, Dong-Hee Lee, Akira Otaka, Ettore Appella, James B. McMahon, Marc C. Nicklaus, Terrence R. Burke Jr., Michael B. Yaffe, Alexander Wlodawer, and Kyung S. Lee.

Correspondence should be addressed to K.S.L. (kyunglee@mail.nih.gov)

Supplementary Methods

Synthesis of F$_2$Pmab-containing mimetic peptide. Synthesis of 2-amino-4,4-difluoro-3-methyl-4-phosphobutanoic acid (F$_2$Pmab)-containing peptides were carried out by employing a *tert*-butoxycarbonyl (Boc)-based solid-phase method on 4-methylbenzhydrylamine (MBHA) resin as described previously[1]. An initial attempt to synthesize a 5-mer PLHS-F$_2$Pmab mimetic peptide did not yield sufficient amounts because of an inefficient coupling of F$_2$Pmab to the resin. Thus, we synthesized a 6-mer F$_2$Pmab-containing peptide (PLHS-F$_2$Pmab-A) and then examined its affinity and specificity to Plk1 in comparison to those of the corresponding p-T78 peptide.

Peptide and GST-PBD pull-down assays. For peptide-based pull-down assays, peptides bearing the N-terminal Cys-(CH$_2$)$_6$ linker (1 mM stock) were cross-linked to the beads using SulfoLink Coupling gel (Pierce, Rockford, IL). For Plk1 pull-down assays with immobilized peptides, we used total cellular lysates prepared from HeLa cells. These cells contain no mutations in the Plk1 coding sequence and express Plk1 at a high level[2]. To prepare mitotic HeLa lysates, cells were treated with 200 ng/ml of nocodazole for 16 h, lysed in TBSN buffer {20 mM Tris-Cl (pH8.0), 150 mM NaCl, 0.5% NP-40, 5 mM EGTA, 1.5 mM EDTA, 0.5 mM Na$_3$VO$_4$, 20 mM *p*-nitrophenyl phosphate, and

protease inhibitor cocktail (Roche, Nutley, NJ)}, and then clarified by centrifugation at 15,000 x g for 20 min at 4°C. The resulting lysates were incubated with the bead-immobilized peptides (40 μM per binding) prepared as above. After incubation for 2 h, peptide-associating proteins were precipitated, washed, and then boiled in sodium dodecyl sulfate (SDS) sample buffer to elute the proteins. Samples were separated by 10% SDS-polyacrylamide gel electrophoresis (PAGE), and then either stained with silver or transferred to PVDF membrane for immunoblotting analysis with anti-Plk1 antibody using the enhanced chemiluminescence (ECL) detection system (Pierce).

To investigate the binding specificity of p-T78 peptides to various Plks, Flag-Plk1 (K82M), Flag-Plk2(K108M)[3] or Flag-Plk3(K52R) (a gift of Wei Dai, New York University School of Medicine, NY) construct was first transfected into HeLa cells. Cellular lysates were prepared as above, mixed, and then incubated in TBSN buffer with the immobilized peptides indicated.

To determine whether PLHSpT binds to the phosphate pincer cleft of the PBD, bead-immobilized PLHSpT or the respective non-phospho PLHST control peptide was incubated with soluble control GST, GST-PBD, or GST-PBD(H538A K540M)[4] for 2 h, washed, and then the precipitated fraction was analyzed.

For p-Cdc25C pull-down assays, either bead-bound GST-PBD or the corresponding GST-PBD(H538A K540M) mutant was incubated with mitotic HeLa lysates in TBSN buffer supplemented with 2 mM DTT. To test the ability of the indicated peptides to compete the PBD-p-Cdc25C interaction, lysates were pre-incubated with GST-PBD for 1.5 h prior to the addition of the indicated peptides. Lysates were then incubated for additional 1.5 h, washed in the binding buffer, and then analyzed. For competition of the interaction between p-Cdc25C and endogenous Plk1, mitotic lysates were prepared in TBSN and incubated with the indicated peptides for 1 h before subjecting to immunoprecipitation with anti-Plk1 antibody.

ELISA-based PBD-binding inhibition assay. A biotinylated p-T78 peptide was first diluted with coating solution (KPL Inc., Gaithersburg, MD) to the final concentration of 0.3 μM, and then 50 μl of the resulting solution was immobilized onto a 96-well streptavidin-coated plate (Nalgene Nunc, Rochester, NY). To block the unoccupied sites, wells were washed once with PBS + 0.05% Tween 20 (PBST) and incubated with 200 μl

of PBS + 1% BSA (blocking buffer) for 1 h. Mitotic 293A lysates expressing HA-EGFP-Plk1[5] were prepared in TBSN buffer. The resulting lysates (60 μg total lysates in 100 μl) were applied onto the biotinylated peptide-coated ELISA wells immediately after mixing with the indicated amount of the competitor peptides, and then incubated with constant rocking for 1 h at 25°C. To terminate the reaction, ELISA plates were washed 4 times with PBST. For detection of the bound HA-EGFP-Plk1, plates were incubated for 2 h with 100 μl/well of monoclonal anti-HA antibody at a concentration of 0.5 μg/ml in the blocking buffer. After washing the plates 5 times, 100 μl of an HRP-conjugated secondary antibody diluted to 1:1000 in the blocking buffer was added onto each well and incubated for 1 h. Afterward, the plates were washed 5 times with PBST and incubated with 100 μl/well of 3,3′,5,5′-Tetramethylbenzidine solution (TMB) (Sigma, St. Louis, MO) as substrate until a desired absorbance was reached. The reactions were terminated by the addition of 1N H_2SO_4 and the optical densities for each sample were measured at 450 nm by using an ELISA plate reader (Molecular Device, Sunnyvale, CA).

Isothermal titration calorimetry analyses. The calorimetric titrations were performed on a VP-ITC titration calorimeter (Microcal, Inc., Northampton, MA). In a typical experiment, 5 μl aliquots of a phosphorylated peptide were injected from a 250 μl syringe into a rapidly mixing (300 rpm) solution of Plk1 PBD (cell volume = 1.3472 ml). Control experiments involved injecting identical amounts of the peptide solution into buffer without Plk1 PBD. The concentrations of Plk1 PBD were 0.033–0.052 mM, and those of the peptides were 0.145–0.365 mM, all concentration values determined by amino acid analysis. Titrations were carried out at 25°C in 20 mM Tris·Cl (pH 7.5), 100 mM NaCl, 3 mM DTT. The isotherms, corrected for dilution/buffer effects, were fit using the Origin ITC Analysis software according to manufacturer's protocols. A nonlinear least-square method was used to fit the titration data and to calculate the errors. Consistent with the structural data, a 1:1 stoichiometry was assumed and the data were fit to a one-site binding model. From the binding curve, values for enthalpy and binding affinity were extracted. Thermodynamic parameters were calculated using $\Delta G = -RT\ln K_a$, $\Delta G = \Delta H - T\Delta S$.

Cloning, Protein Expression, and Purification. Two forms of Plk1 PBD (residues 326-603 and residues 367-603) were expressed as fusion constructs with an N-terminal

3

His$_6$-DsRed tag in a vector based on pDEST-527 (Addgene, Cambridge, MA). Another form of Plk1 PBD (residues 371-603) was expressed with an N-terminal His$_6$-MBP tag in a vector based on pET-28a (Novagen, Madison, WI). A TEV protease cleavage site was engineered between the tag and PBD. The vectors were expressed in either *E. coli* BL21(DE3)pLysS or Rosetta 2 cells (Novagen) with similar yield. Cells were grown to an optical density of 0.4 at 30°C with vigorous shaking. The cultures were cooled to 20°C, induced by addition of IPTG to a final concentration of 0.4 mM, and incubated for 12 h. The cells were harvested and the pellets were frozen prior to lysis. All subsequent purification was done at 4°C. The frozen pellets were thawed in buffer A (20 mM Tris-Cl, pH 8.0, 500 mM NaCl, 3 mM DTT) and lysed by addition of 4% v/v BugBuster 10X protein extraction reagent (Novagen) and 0.1 mg/ml of DNase I (Sigma). The lysate was centrifuged at 40000 x g for 30 minutes to pellet the cell debris and filtered through a 0.2 µm filter. The lysate was loaded onto HisTrap HP columns (Amersham Biosciences, Piscataway, NJ) with 100 mM imidazole, washed with 100 mM imidazole in buffer A, and eluted with 500 mM imidazole in buffer A. The peaks containing the fusion protein were digested with TEV protease (1:100 molar ratio) overnight by dialysis against buffer A. The digestion was reloaded onto HisTrap HP column without imidazole, washed with buffer A, and eluted with 80 mM imidazole in buffer A. A HiLoad 16/60 Superdex 75 gel filtration column (Amersham) equilibrated with buffer A was used as the final step in purification. Full length PBD was dialyzed against a low salt buffer (20 mM Tris·Cl, pH 7.5, 100 mM NaCl, 3 mM DTT), and used in calorimetry experiments. The truncated forms of PBD were used for crystallography. The kinase domain of Plk1 (residues 1-337) was purified in the same manner. His$_6$-MBP constructs were purified by Ni metal affinity chromatography, loaded on to an amylose-agarose column, and then eluted with 50 mM maltose in a buffer {10 mM Tris (pH 8), 0.5 M NaCl, 2 mM DTT}. The resulting protein was digested with TEV protease to cleave the tag, flowed through Ni column, and then finally subjected to gel filtration. The PBD of human Plk2 (residues 373 to 685) was cloned as a MBP fusion with a TEV protease cleavage site and purified as the same fusion with PBD of Plk1.

Crystallization, Data Collection, and Refinement for PBD^{LH}. Crystals of the Plk1 PBD-LHSpTA complex were grown by hanging drop vapour diffusion using 1 µl of

protein solution (12 mg/ml in 10 mM Tris-Cl, pH 8.0, 0.5 M NaCl, 10 mM DTT, 2 mM Ac-LHSpTA-NH$_2$ peptide) mixed with 1 μl of well solution consisting of 32.5% PEG 2000 MME, 0.1 M Tris-Cl, pH 8.5, 0.2 M trimethyl-amine N-oxide. Crystals grew overnight at room temperature. For data collection, a crystal was looped from the drop and flash frozen by direct transfer to a cryostream at 100 K. Data was collected with a rotating anode home source on a Rigagku R-axis IV detector and processed using the HKL2000 package[6]. A molecular replacement solution was found with AMoRe[7]. Initial refinement was done with CNS 1.21[8] with manual model fitting using XtalView[9]. The final rounds of refinement were completed in PHENIX 1.3[10] with the addition of riding hydrogens.

Cell culture and microinjection. HeLa cells were cultured as subconfluent monolayers under the conditions recommended by American Type Culture Collection (Manassas, VA). To acutely inhibit the Cdc2 kinase activity, HeLa cells arrested with 200 ng/ml of nocodazole for 16 h were treated with 200 nM of BMI-1026 for 10 min. No mitotic exit was observed during the period of BMI-1026 treatment (data not shown). For microinjection experiments with the Pmab-containing mimetic peptides, cells were arrested with 2.5 mM thymidine (Sigma) for 16 h and released into fresh medium. Two hours after release from the S phase block, the indicated peptides (2.5 mM stock in PBS) were microinjected into the cells using Eppendorf Transjector 5246 (Eppendorf, Westbury, NY) at the 150 hPa pressure level and the 0.5 second injection time. All the cells in a single grid were injected and then further incubated to monitor cell cycle progression. For microinjection experiments with the F$_2$Pmab-containing mimetic peptides, cells were arrested with 2.5 mM thymidine for 16 h twice with a 9 h release interval, and then released into fresh medium. Seven hours after release from the G1/S phase block, the indicated peptides (4 mM stock in PBS) were microinjected similarly as above. Where indicated, peptides containing the final concentration of 30 ng/μl of pEGFP-C1 vector (Clontech, Mountain View, CA) were used to visualize the injected cells.

To determine the level of Plk1 delocalization by the microinjected PLHS-Pmab peptide, cells were released for 5 h from the single thymidine (S phase) block and then

microinjected as above. Four hours after microinjection, cells were fixed and subjected to immunostaining analyses as described below.

Electroporation. For the purpose of investigating a long term effect of the peptide, a 6-mer Biotin-conjugated p-T78 mimetic peptide {Biotin-$(CH)_6$-PLHS-F_2Pmab-A-NH_2} was electroporated into asynchronously growing HeLa cells using a Bio-Rad Gene Pulser (Bio-Rad Laboratories, Hercules, CA) at 250 μFD and 300 V. Cells were then incubated for 2 days, fixed, and then subjected to immunostaining analysis.

Indirect immunofluorescence and confocal microscopy. Indirect immunostaining was carried out as described previously[5] using anti-Plk1 antibody (Santa Cruz Biotechnologies, Santa Cruz, CA) and anti-CREST antiserum (Cortex Biochem, San Leandro, CA). All the appropriate secondary antibodies used for this study were purchased from Invitrogen (Carlsbad, CA). Biotinylated F_2Pmab-positive cells were detected by co-staining with FITC-conjugated Streptavidin (Invitrogen). Chromosomes were visualized with 4',6-diamidino-2-phenylindole (DAPI) (Sigma). Digital images were collected with a Zeiss LSM510 confocal microscope. For the quantification of the fluorescence signal intensities, images of unsaturated fluorescence signals were acquired with the same laser intensity at 512×512 pixels and 12-bit resolution. Fluorescence intensities for localized signals were determined after subtracting the background signal intensities using Zeiss AIM confocal software.

Accession codes. Protein Data Bank: Coordinates for PBD^{LH} has been deposited with accession code 3FVH.
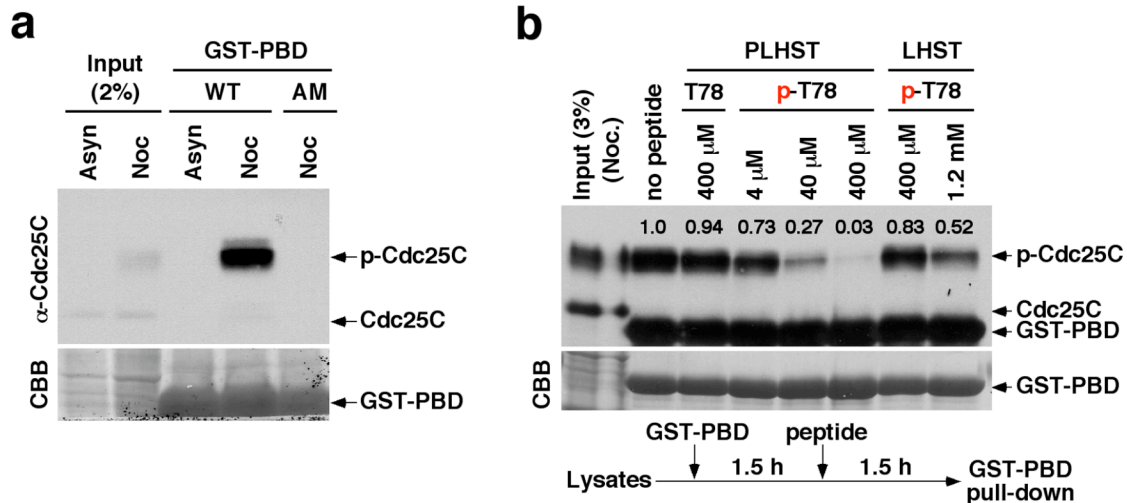
Supplementary Figure 1
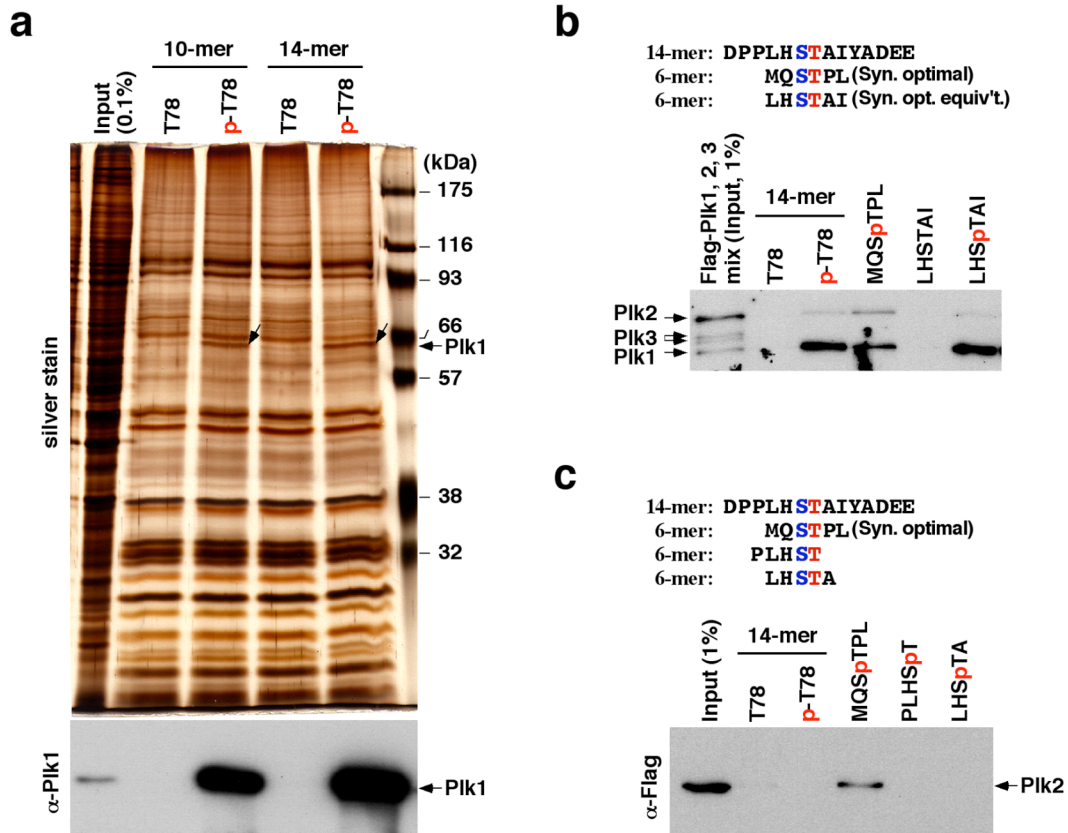
Supplementary Fig. 1. p-T78 peptides, but not a synthetic optimal peptide, exhibit a high level of Plk1 PBD-binding specificity. **(a)** p-T78 peptides, but not the respective non-phospho forms, precipitate Plk1 as the major binding protein from mitotic HeLa lysates. Mitotic lysates were prepared in TBSN buffer containing 20 mM *p*-nitrophenyl phosphate to inhibit dephosphorylation of p-T78 peptides. The resulting lysates were incubated with bead-immobilized non-phospho T78 (T78) or p-T78 peptides (10-mer and 14-mer) shown in **Fig. 1a**. Bead-associated proteins were separated in 10 % SDS-PAGE, and stained with silver (**Top**) or immunoblotted with anti-Plk1 antibody (**Bottom**). Arrows, Plk1 precipitated with p-T78 peptides. **(b)** A 6-mer p-T78 peptide (LHSpTAI) analogous to the synthetic optimal peptide (MQSpTPL) preferentially precipitates Plk1, whereas MQSpTPL binds to both Plk1 and, at a reduced level, Plk2. The mixture of HeLa lysates expressing the kinase-inactive Plk1(K82M), Flag-Plk2(K108M), or Flag-Plk3(K52R) was incubated with the indicated peptides cross-linked to the beads. Precipitates were washed, separated, and then subjected to immunoblotting analysis with

7

anti-Flag antibody. **(c)** The synthetic optimal PBD-binding peptide (MQSpTPL) [4] binds to Plk2. HeLa lysates expressing Flag-Plk2 were incubated with the immobilized peptides indicated under the conditions described in the Materials and Methods. Precipitates were analyzed as in **Fig. 2a**.

Supplementary Figure 2

Supplementary Fig. 2. Concentration-dependent inhibition of the Plk1-p-Cdc25C interaction by minimal p-T78 peptides. **(a)** Either asynchronous (Asyn) or mitotic (Noc) HeLa lysates were incubated with bacterially-expressed GST-PBD or the GST-PBD(H538A K540M) mutant. GST-PBD-binding proteins were precipitated, washed, and then blotted with anti-Cdc25C antibody. The same membrane was stained with Coomassie (CBB). **(b)** Mitotic HeLa lysates were pre-incubated with bead-bound GST-PBD for 1.5 h before the addition of the peptides at the concentrations indicated. After additional 1.5 h incubation, GST-PBD-binding proteins were precipitated and analyzed as in **(a)**. Although less effective than PLHSpT, LHSpT also interfered with the PBD-p-Cdc25C interaction. GST-PBD was detected in the anti-Cdc25C blot as a result of previous immunoblotting with anti-GST antibody. Numbers indicate relative efficiency of the p-Cdc25C pull-down by GST-PBD.
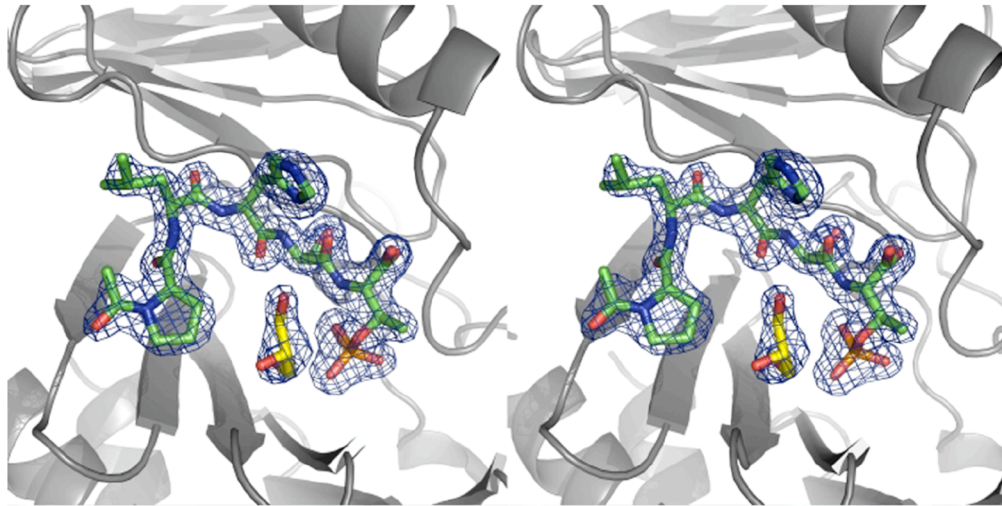
Supplementary Figure 3
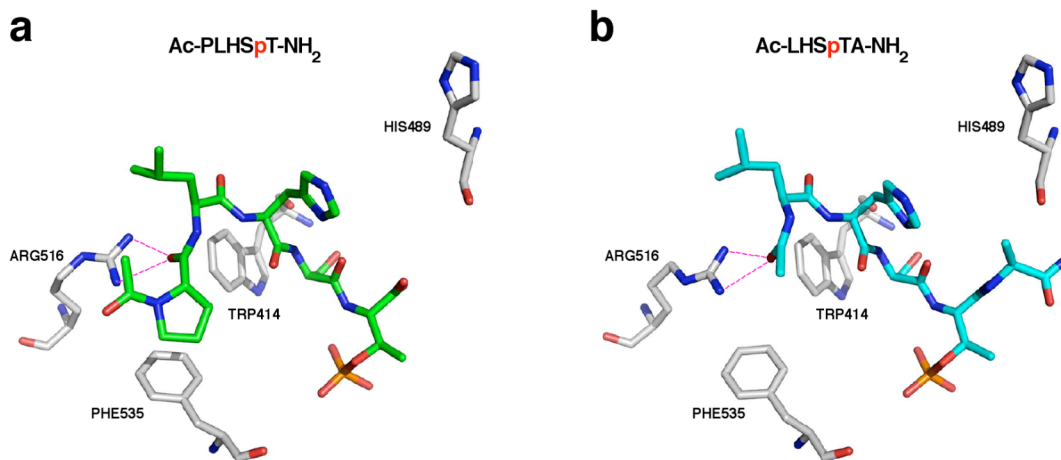
Supplementary Fig. 3. Comparative analyses on the structures of the PBD in complex with Ac-PLHSpT-NH$_2$ or Ac-LHSpTA-NH$_2$. The core PBD-binding mode for Ac-LHSpTA-NH$_2$ and Ac-PLHSpT-NH$_2$ remains largely the same. It is noteworthy that, in the Ac-PLHSpT-NH$_2$ structure, the carbonyl oxygen of the peptide bond between the Pro-4 and the Leu-3 is hydrogen-bonded to the guanidinium moiety of Arg516 of PBD (two red dotted lines). Similarly, by mimicking a peptide bond in the non-terminal regions of any peptide or protein, the N-terminal acetyl carbonyl oxygen in Ac-LHSpTA-NH$_2$ is in hydrogen bond with Arg516 (two red dotted lines). Notably, the PBDs from both Plk2 and Plk3 possess the Lys and Tyr residues at the positions analogous to the Arg516 and Phe535, respectively, of Plk1 PBD, suggesting that the Arg516 and Phe535 residues are likely important for Plk1 PBD-binding specificity. Since both Ac-PLHSpT-NH$_2$ and Ac-LHSpTA-NH$_2$ exhibited a high Plk1 specificity, the hydrogen bond generated between the carbonyl oxygen N-terminal to Leu-3 and the guanidinium moiety of Arg516 of Plk1 PBD could be critical for achieving the Plk1 specificity. The role of F535 in attaining Plk1 specificity has not been determined. However, mutations of the analogous Lys and Tyr residues in Plk2 and Plk3 to Arg and Phe, respectively, {i. e., Plk2(K607R, Y626F) and Plk3(K568R, Y587F) mutations} failed to enhance the ability of Plk2 and Plk3 to bind to the synthetic optimal peptide (MQSpTPL). Rather, they eliminated the moderate level of the interaction normally observed between Plk2 and the latter peptide. These observations suggest that a broader primary sequence context of the PBD is likely important in properly forming the phosphopeptide-binding module and

9

preserving the overall structural integrity of the PBD. PDB ID for PBD^{PL}, 3HIK; PDB ID for PBD^{LH}, 3FVH.

Supplementary Figure 4

Supplementary Fig. 4. Stereo image of the PBD phosphopeptide-binding pocket. PLHSpT is drawn in green and the neighboring glycerol in the binding pocket of PBD^{PL} is in yellow. The 2|F$_o$|-|F$_c$| electron density is contoured to 1.5 σ around PLHSpT and its associated glycerol molecule in blue mesh. PDB ID for PBD^{PL}, 3HIK.
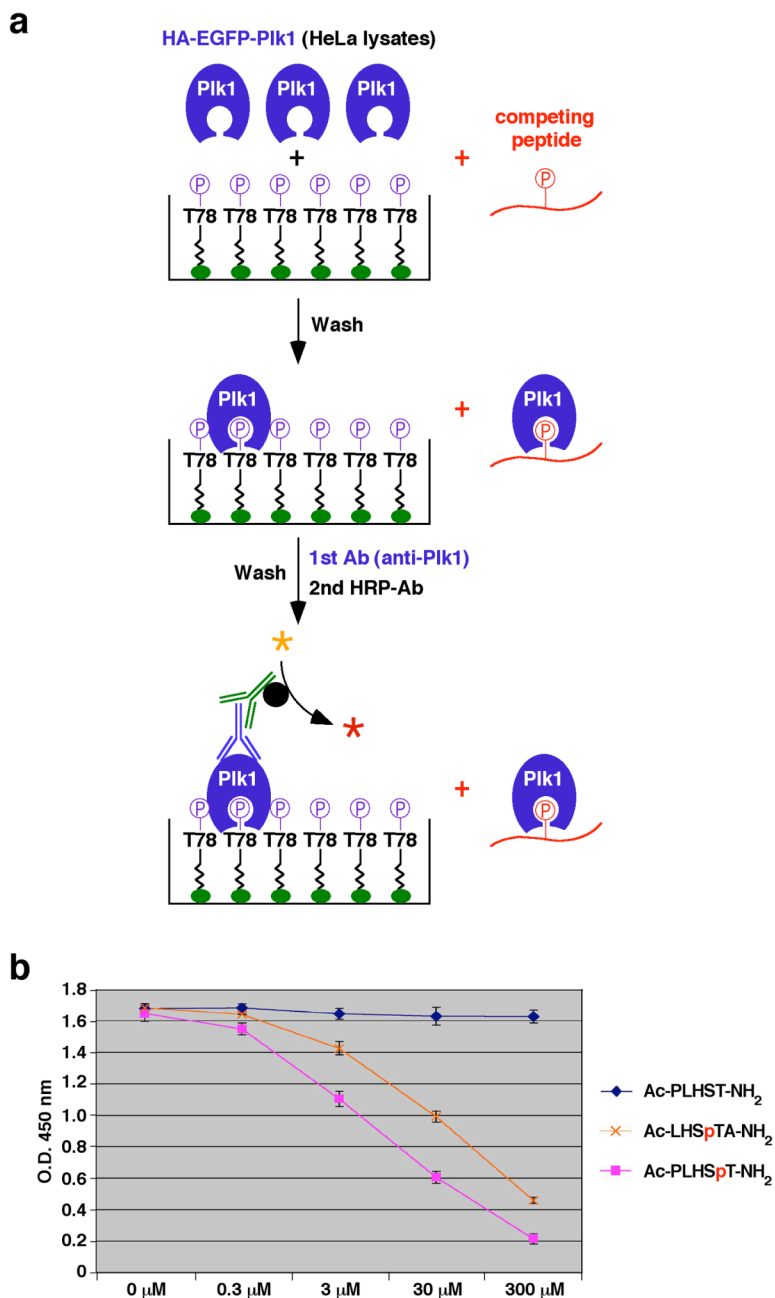
Supplementary Figure 5
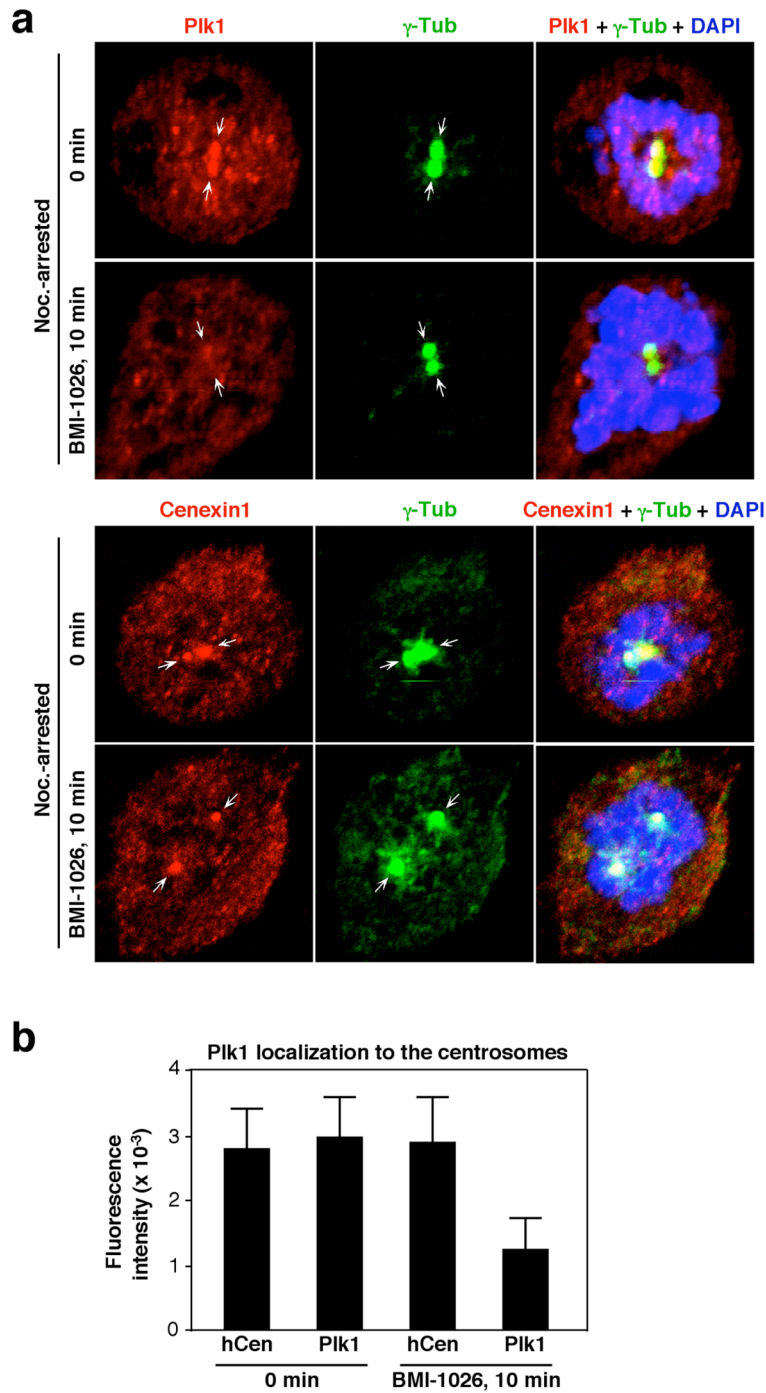
Supplementary Fig. 5. Acute inhibition of Cdc2 activity induces Plk1 delocalization from the centrosomes. **(a)** Mitotic HeLa cells were prepared by the addition of 100 ng/ml of a microtubule-depolymerizing drug, nocodazole, for 16 h. The resulting cells were further treated with 200 nM of a Cdc2 inhibitor, BMI-1026[11], for 10 min, fixed and then

immunostained with anti-Plk1 and anti-γ-tubulin antibodies **(Top)** or anti-hCenexin1 and anti-γ-tubulin antibodies **(Bottom)**. Cells did not exit from mitosis during the 10 min treatment, as evidenced by the pre-anaphase chromosomal DNA morphology. Inhibition of Cdc2 activity greatly diminished the level of centrosomal Plk1 signals, whereas it did not significantly alter the level of another centrosomal protein, hCenexin1. Since Cdc2 is one of the major priming kinases for the PBD-binding sites, these observations suggest that disruption of the PBD-dependent protein-protein interaction is sufficient to impair Plk1 localization and therefore its function. The γ-tubulin signals mark the position of centrosomes. Arrows, centrosomes. **(b)** Quantification of the centrosome fluorescence intensities for Plk1 and hCenexin1 was carried out as described in the Methods.
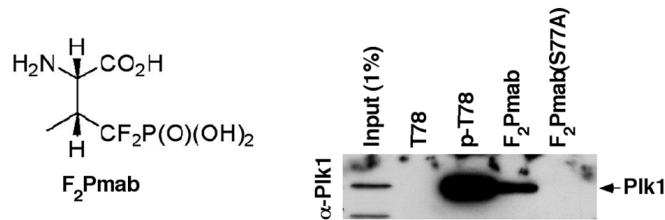
Supplementary Figure 6

Supplementary Fig. 6. Comparative analyses of the PBD inhibition by two minimal p-T78 peptides, Ac-PLHSpT-NH$_2$ and Ac-LHSpTA-NH$_2$. **(a)** Schematic diagram illustrating the PBD-binding inhibition assay. Biotinylated p-T78 peptides (green dots with wiggled p-T78 peptide) were immobilized on the avidin-coated ELISA wells, and then incubated with HeLa lysate expressing HA-EGFP-Plk1 in the presence of a competitor peptide (red). After incubation, plates were washed and the level of HA-

EGFP-Plk1 bound to the biotinylated peptide was quantified by incubating the ELISA wells with anti-HA antibody (blue), followed by HRP-conjugated secondary antibody (the green antibody with a black dot). The yellow and red asterisks indicate 3,3′,5,5′-Tetramethylbenzidine (TMB) substrate and its reaction product, respectively, generated by HRP. **(b)** To determine the efficiency of the PBD inhibition by the indicated peptide, the HA-EGFP-Plk1-expressing HeLa lysates were added onto the ELISA wells immediately after mixing with various amounts of the peptide. Ac-PLHSpT-NH$_2$ exhibited a higher level of PBD inhibition than Ac-LHSpTA-NH$_2$, suggesting that the Pro-4-dependent hydrophobic interactions of Ac-PLHSpT-NH$_2$ with the Trp414 and Phe535 residues as shown in **Supplementary Fig. 3** are stronger than the van der Waals contacts generated by the Ala+1 residue in Ac-LHSpTA-NH$_2$. Bars, standard deviation.
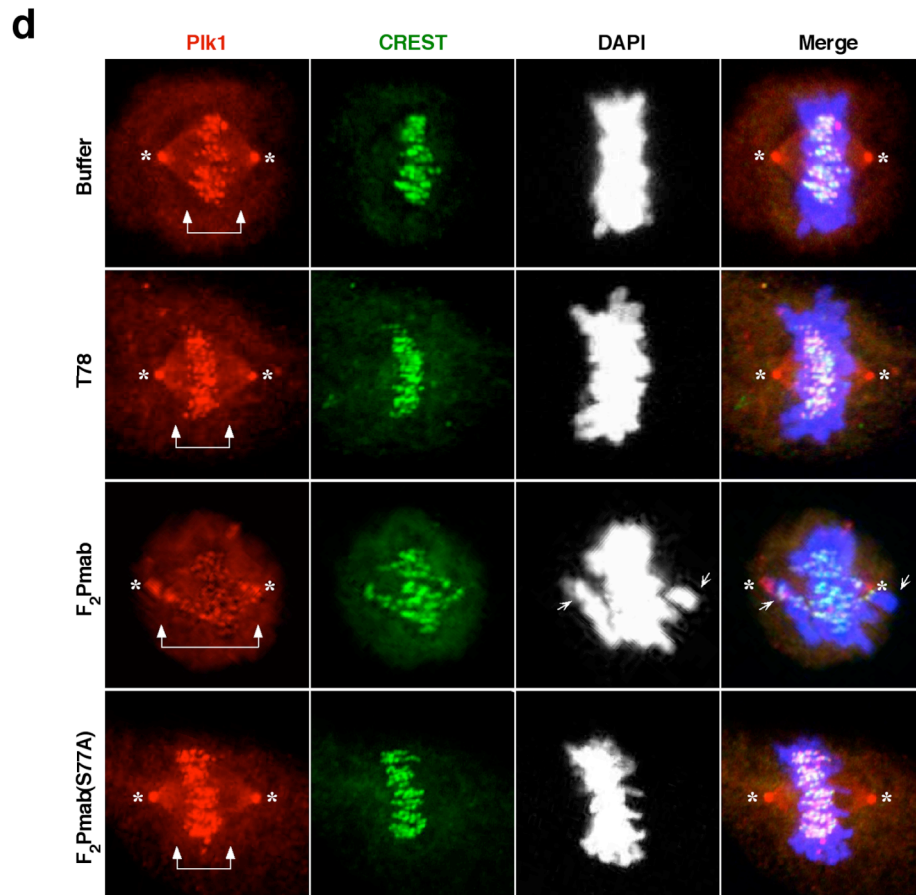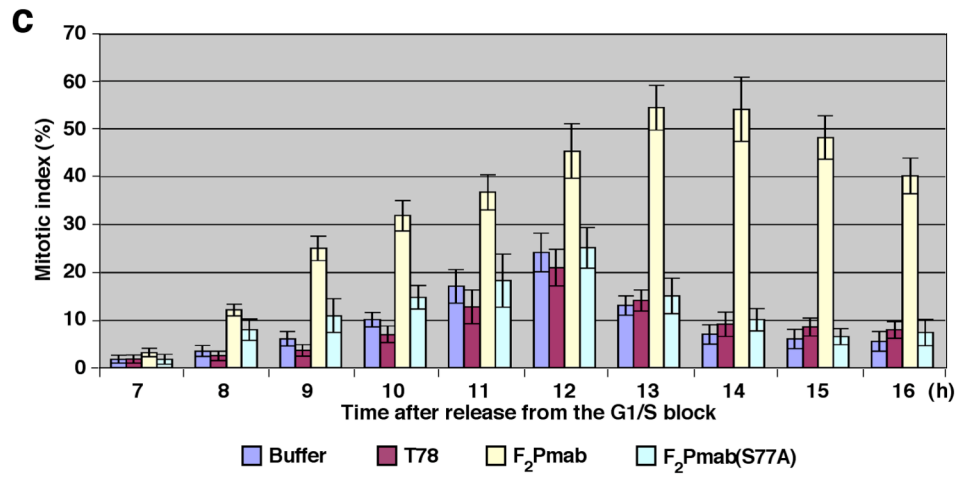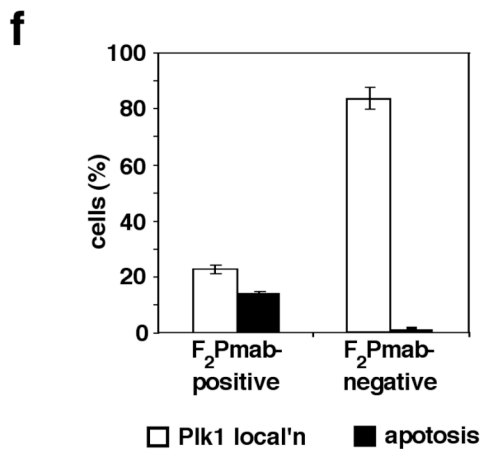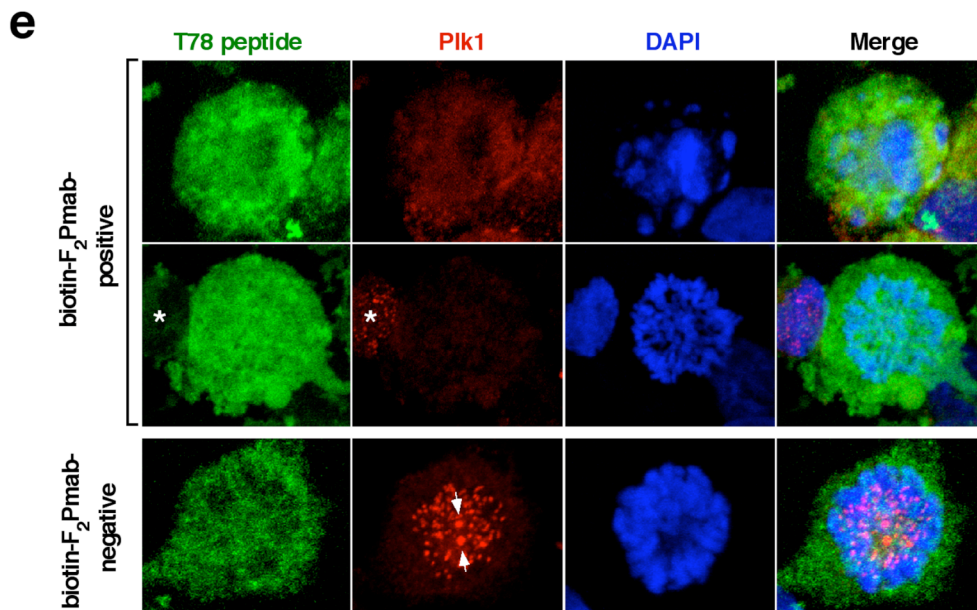
Supplementary Figure 7a,b

a

b
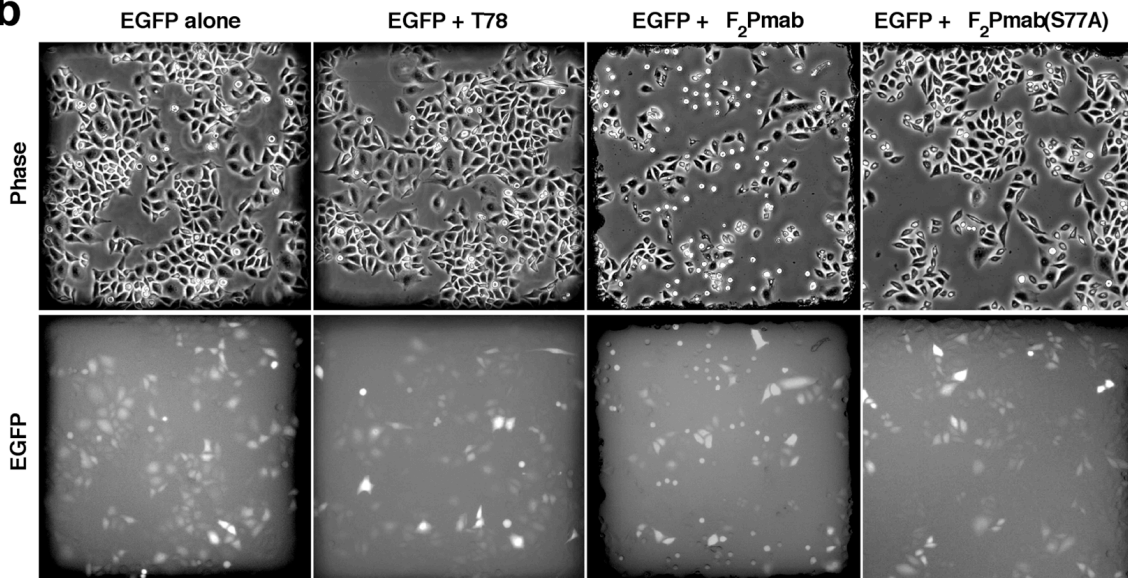
Supplementary Figure 7c,d

Supplementary Figure 7e,f

Supplementary Fig. 7. A 6-mer, p-T78 mimetic, peptide (PLHS-F$_2$Pmab-A), but not the respective PLHA-F$_2$Pmab-A mutant, induces a mitotic arrest and apoptotic cell death in HeLa cells. **(a)** Illustration of a nonhydrolyzable p-Thr derivative, F$_2$Pmab **(Left)**, used for the synthesis of mimetic peptides. The indicated peptides cross-linked to the beads were incubated with mitotic HeLa lysates in the presence of phosphatase inhibitors, precipitated, and then analyzed as in **Fig. 1a**. The immobilized C-(CH$_2$)$_6$-PLHS-F$_2$Pmab-A peptide (F$_2$Pmab), but not the C-(CH$_2$)$_6$-PLHA-F$_2$Pmab-A mutant {in short, F$_2$Pmab(S77A)}, precipitated Plk1 at a level a few fold lower than that of the control C-

(CH$_2$)$_6$-PLHSpTA peptide. **(b,c)**, Cells were arrested at the G1/S boundary by double thymidine treatment and then released into fresh medium. Seven hours after release, all the cells in a single grid were microinjected with a mixture containing 4 mM of the indicated peptides and 30 ng/µl of pEGFP-C1 vector, and then further incubated. Cells were photographed 16 h after G1/S release (9 h after microinjection) **(b)**. The co-injected green fluorescent EGFP plasmid served as a convenient indicator for assessing the level of microinjected peptides. Among the cells microinjected with PLHS-F$_2$Pmab-A, a majority of the EGFP-positive cells were rounded-up. Reduction in the total cell number in **(c)** was the result of loss of floating dead cells. The percentages of mitotic cells were quantified at the indicated time points to monitor cell cycle progression. Bars, standard deviation. **(d)** Cells at the 13 h time point in **(c)** were co-stained with anti-Plk1 antibody and anti-CREST antiserum. Asterisks, centrosome-localized Plk1 signals; Arrowed brackets, kinetochores-localized Plk1 signals; barbed arrows, misaligned chromosomes. **(e,f)**, Electroporation of HeLa cells with the F$_2$Pmab-bearing peptide leads to Plk1 delocalization and apoptotic cell death. HeLa cells were electroporated with biotinylated PLHS-F$_2$Pmab-A peptide (biotin-F$_2$Pmab). Two days after electroporation, cells were stained with FITC-streptavidin and anti-Plk1 antibody to determine the biotin-F$_2$Pmab-positive and biotin-F$_2$Pmab-negative cells **(e)**. Among these populations, cells exhibiting proper Plk1 localization or apoptotic chromosome morphology were quantified **(f)**. An asterisk in **(e)** indicates a poorly electroporated (weak biotin-F$_2$Pmab) cell that displays localized Plk1 signals. Arrows indicate centrosomes.

Supplementary Table 1. Peptides used for this study

Length	Peptides [a]	Source
Linker phospho-forms		
14 mer	NH_2-C-$(CH_2)_6$-DPPLHS**pT**AIYADEE-NH_2	This study
10-mer	NH_2-C-$(CH_2)_6$-PLHS**pT**AIYAD-NH_2	This study
9-mer	NH_2-C-$(CH_2)_6$-PLHS**pT**AIYA-NH_2	This study
8-mer	NH_2-C-$(CH_2)_6$-PLHS**pT**AIY-NH_2	This study
7-mer	NH_2-C-$(CH_2)_6$-PLHS**pT**AI-NH_2	This study
6-mer	NH_2-C-$(CH_2)_6$-PLHS**pT**A-NH_2	This study
5-mer	NH_2-C-$(CH_2)_6$-PLHS**pT**-NH_2	This study
4-mer	NH_2-C-$(CH_2)_6$-LHS**pT**-NH_2	This study
3-mer	NH_2-C-$(CH_2)_6$-HS**pT**-NH_2	This study
2-mer	NH_2-C-$(CH_2)_6$-S**pT**-NH_2	This study
6-mer	NH_2-C-$(CH_2)_6$-LHS**pT**AI-NH_2	This study
5-mer	NH_2-C-$(CH_2)_6$-LHS**pT**A-NH_2	This study
4-mer	NH_2-C-$(CH_2)_6$-HS**pT**A-NH_2	This study
5-mer	NH_2-C-$(CH_2)_6$-HS**pT**AI-NH_2	This study
4-mer	NH_2-C-$(CH_2)_6$-S**pT**AI-NH_2	This study
5-mer	NH_2-C-$(CH_2)_6$-PAHS**pT**-NH_2	This study
5-mer	NH_2-C-$(CH_2)_6$-PPHS**pT**-NH_2	This study
5-mer	NH_2-C-$(CH_2)_6$-PQHS**pT**-NH_2	This study
5-mer	NH_2-C-$(CH_2)_6$-PLQS**pT**-NH_2	This study
5-mer	NH_2-C-$(CH_2)_6$-PQQS**pT**-NH_2	This study
5-mer	NH_2-C-$(CH_2)_6$-MLHS**pT**-NH_2	This study
6-mer	NH_2-C-$(CH_2)_6$-MQS**pT**PL-NH_2	[4]
9-mer	Biotin-C-$(CH_2)_6$-$(CH_2)_6$-DPPLHS**pT**AI-NH_2	This study
Linker non-phospho forms		
14 mer	NH_2-C-$(CH_2)_6$-DPPLHS**T**AIYADEE-NH_2	This study
10-mer	NH_2-C-$(CH_2)_6$-PLHS**T**AIYAD-NH_2	This study
6-mer	NH_2-C-$(CH_2)_6$-LHS**T**AI-NH_2	This study
6-mer	NH_2-C-$(CH_2)_6$-PLHS**T**A-NH_2	This study
5-mer	NH_2-C-$(CH_2)_6$-PLHS**T**-NH_2	This study
Linker p-T78 mimetic forms		
5-mer	NH_2-C-$(CH_2)_6$-PLHS-**Pmab**-NH_2	This study
5-mer	NH_2-C-$(CH_2)_6$-PLHA-**Pmab**-NH_2	This study
6-mer	NH_2-C-$(CH_2)_6$-PLHS-**F_2Pmab**-A-NH_2	This study
6-mer	NH_2-C-$(CH_2)_6$-PLHA-**F_2Pmab**-A-NH_2	This study
6-mer	Biotin-$(CH_2)_6$-PLHS-**F_2Pmab**-A-NH_2	This study
No linker forms (p-T78, T78, and mimetic)		
5-mer	Ac-PLHS**pT**-NH_2	This study
4-mer	Ac-LHS**pT**-NH_2	This study
5-mer	Ac-LHS**pT**A-NH_2	This study
4-mer	Ac-HS**pT**A-NH_2	This study

18

5-mer	Ac-PLHS**T**-NH$_2$	This study
4-mer	Ac-LHS**T**A-NH$_2$	This study
6-mer	Ac-PLHS**T**A-NH$_2$	This study
5-mer	Ac-PLHS-**Pmab**-NH$_2$	This study
5-mer	Ac-PLHA-**Pmab**-NH$_2$	This study
6-mer	Ac-PLHS-**F$_2$Pmab**-A-NH$_2$	This study
6-mer	Ac-PLHA-**F$_2$Pmab**-A-NH$_2$	This study

[a] The p-T78 and T78 residues, and the phospho-Thr mimetic Pmab and F$_2$Pmab are marked in red.

19

Supplementary References

1. Otaka, A., Mitsuyama, E., Kinoshita, T., Tamamura, H. & Fujii, N. Stereoselective synthesis of CF(2)-substituted phosphothreonine mimetics and their incorporation into peptides using newly developed deprotection procedures. *J. Org. Chem.* **65**, 4888-4899. (2000).

2. Simizu, S. & Osada, H. Mutations in the Plk gene lead to instability of Plk protein in human tumour cell lines. *Nat. Cell Biol.* **2**, 852-854. (2000).

3. Ma, S., Liu, M.A., Yuan, Y.-L. & Erikson, R.L. The serum-inducible protein kinase Snk is a G1 phase polo-like kinase that is inhibited by the calcium- and integrin-binding protein CIB. *Mol. Cancer Res.* **1**, 376-384. (2003).

4. Elia, A.E. et al. The molecular basis for phospho-dependent substrate targeting and regulation of Plks by the polo-box domain. *Cell* **115**, 83-95. (2003).

5. Seong, Y.S. et al. A spindle checkpoint arrest and a cytokinesis failure by the dominant-negative polo-box domain of Plk1 in U-2 OS cells. *J. Biol. Chem.* **277**, 32282-32293. (2002).

6. Otwinowski, Z. & Minor, W. Processing of X-ray diffraction data collected in oscillation mode. . *Methods Enzymol.* **276**, 307-326. (1997).

7. Navaza, J. AMoRe: an automated package for molecular replacement. *Acta Cryst.* **A50** 157-163. (1994).

8. Brunger, A.T. Version 1.2 of the Crystallography and NMR system. *Nat. Protoc.* **2**, 2728-2733. (2007).

9. McRee, D.E. XtalView/Xfit--A versatile program for manipulating atomic coordinates and electron density. *J. Struct. Biol.* **125**, 156-165. (1999).

10. Adams, P.D. et al. PHENIX: building new software for automated crystallographic structure determination. *Acta Crystallogr. D. Biol. Crystallogr.* **58**, 1948-1954. (2002).

11. Seong, Y.S. et al. Characterization of a novel cyclin-dependent kinase 1 inhibitor, BMI-1026. *Cancer Res.* **63**, 7384-7391. (2003).